# AEROACOUSTIC PHENOMENA IN HIGH-PRESSURE CENTRIFUGAL COMPRESSORS—A POSSIBLE ROOT CAUSE FOR IMPELLER FAILURES

by
**Sven König**
**Research Engineer**

**Nico Petry**
**Scientific Assistant**
**and**
**Norbert G. Wagner**
**Siemens Energy Sector**
**Oil & Gas Division**
**Duisburg, Germany**

*Sven König is a Research Engineer within Siemens Energy Sector, Oil & Gas Division, Duisburg, Germany. His main fields of interest are rotor/stator interactions and aeroacoustic phenomena in centrifugal compressors. Dr. König has authored several conference and journal papers in the field of unsteady turbomachinery aerodynamics, and, more recently, on excitation mechanisms in centrifugal compressors.*

*Dr. König Studied Mechanical Engineering at the Technical University Kaiserslautern/Germany and the University of California/Irvine. He received a M.Sc. degree from TU Kaiserslautern in 2001. In 2006 he received a Ph.D. degree from Technical University Darmstadt in cooperation with Texas A&M University.*

*Nico Petry is a Scientific Assistant doing his Ph.D. at Siemens Energy Sector, Oil & Gas Division, Duisburg, Germany. His research project on unsteady phenomena and excitation mechanisms in centrifugal compressors is being carried out in close cooperation with the Institute of Energy and Environmental Engineering (Turbomachinery division) of the University Duisburg/Essen, Germany.*

*Mr. Petry studied Mechanical Engineering at University Duisburg Essen and received his diploma in 2007.*

*Norbert G. Wagner is Head of Component Development within Siemens Energy Sector, Oil & Gas Division, Compressor Product Development, in Duisburg, Germany. In this capacity, he is responsible for the basic technologies. He has worked in particular on dynamic coefficients of labyrinth seals and he has authored several papers on rotordynamics of high-pressure applications.*

*Dr. Wagner received his Diplom degree in 1981 from the University of Duisburg and his doctorate from Technical University of Darmstadt in 2000.*

## ABSTRACT

During the past decades studies of aeroacoustic phenomena in turbomachinery were mainly carried out by research institutions. The aerospace industry was the main driver in this field since noise issues gained more and more significance. Though it has been known for some years that acoustic resonances may also lead to strong excitation sources, very little is known about the relevant physics, especially for centrifugal compressors. Failures that were observed in the field could not be explained by state-of-the-art analysis procedures, and it became clear from customer discussions that there is a strong need for better understanding of aeroacoustic excitation mechanisms; these were suspected to play a significant role in the root causes of the failures. To improve the reliability of centrifugal compressors, especially for high-pressure applications, an extended in-house research program has been launched to better understand the involved interactions that may lead to machine failures. The current paper gives an overview on the research activities, presents the underlying theory, and gives new results that are relevant from a practical point of view. A new aeroacoustic excitation model is presented and its successful application to explain two impeller failures in the oil and gas industry is illustrated.

## INTRODUCTION

When talking about acoustics in an industrial context, one usually refers to the noise emitted by mechanical systems. A silencer may be the suitable solution for the emitted noise. However, the situation changes dramatically if acoustic resonances occur within the machine, e.g., within a compressor. In such a case the pressure fluctuations may reach very high levels, even jeopardizing safe operation of the whole facility. Of course, such conditions are unacceptable to the operator, since a shutdown or even a failure of the compressor may easily cost hundreds of thousands of dollars. The costs for a shutdown are especially high in the oil and gas industry, where it is expected that the facility will run nonstop, except for maintenance intervals. On the way toward increasing operational availability aeroacoustic mechanisms must be taken into account and a profound understanding of the relevant mechanisms is crucial.

Looking at the available literature, investigations on acoustic phenomena in turbomachinery were mainly focused on axial machines. In their milestone paper in 1961 Tyler and Sofrin (1961) discussed rotor/stator-interaction and the resulting spinning modes for an axial-flow compressor. The study was focused on noise; however, the rotating pressure patterns resulting from the interaction between rotating and stationary components (referred to as

Tyler/Sofrin modes) may also constitute a strong excitation source—characterized by the blade-passing frequency. In the field of axial turbomachinery this basic study was followed by a number of papers, but very few publications are available for centrifugal compressors. One case where a compressor failure was reported can be found in the two-part paper by Eckert (1999) and Ni (1999). According to their analysis the shroud disk of a radial fan impeller failed due to aeroelastic self-excitation. Ziada, et al. (2002), studied an acoustic resonance in the inlet scroll of a turbocompressor. They delivered a root cause for high vibration levels, triggered by the interaction between vortex shedding and a standing wave in the ring chamber. Franke, et al. (2005), investigated rotor/stator interactions and the resulting mode shapes in a reversible radial-pump turbine. Eisinger (2002) and Eisinger and Sullivan (2002) presented a basic approach to evaluate critical resonance conditions caused by acoustic modes. Focus was given on the coupling between acoustic and structural modes. A different excitation source in turbomachinery, also associated with acoustic modes, was investigated by Parker, et al., in a series of studies (Parker, 1967a, 1967b, 1984; Parker and Pryce, 1974; Parker and Stoneman, 1985, 1987). Parker, starting with fundamental investigations on flat plates, could show that the vortices shed from the trailing edges of compressor blades can excite acoustic resonances between the blades. The resulting modes are characterized by different mode shapes $\alpha$, $\beta$, $\gamma$ and $\delta$ and are referred to as *Parker modes*. Those modes are localized between the blades and only occur for sufficiently high chord-to-pitch ratios.

Reviewing the available literature it is obvious that there is a lack of understanding concerning aeroacoustic and aeroelastic phenomena in centrifugal compressors. Papers on noise issues and silencer solutions for centrifugal compressors are available, but not reviewed in the current paper, since they are not related to impeller excitation. To gain insight into the complex interaction mechanisms that may lead to impeller excitation, the authors' company in Duisburg has launched an extended in-house research program, which covers different aspects of flow-induced excitation phenomena for centrifugal compressors. As a first step, the acoustics, fluid dynamics, and mechanics of the system are treated separately, using analytical, numerical, and experimental approaches. Petry, et al. (2009), presented first results of this research program, with special focus on rotor/stator interaction and impeller excitation. If the pressure patterns due to rotor/stator interaction excite acoustic eigenmodes in the connecting cavities, resonances may lead to high levels of noise, and, more importantly, vibration amplitudes that may, under certain conditions, ultimately lead to machine failures. A recent numerical study by König (2009) covers the aspect of acoustic eigenmodes in the side cavities of centrifugal compressors. The study revealed that a high modeling effort may be necessary to obtain reliable cavity eigenfrequencies.

In general, any cavity may act as an acoustic resonator. Considering the complex geometry of a turbocompressor, it is obvious that it is quite a challenge to assess the different cavities that are relevant in terms of possible excitation sources. Critical operating conditions occur when the acoustic eigenfrequencies are excited—usually by the unsteadiness of the flow—and the frequency of the establishing acoustic mode matches the natural frequency of the confining structure. Moreover, the mode shapes of structure and acoustic mode must be similar for a coupling between acoustic mode and structure to occur. Of course, it is of importance to identify all possible excitation sources that may trigger the acoustic resonance. In the present paper a survey on the various excitation sources like Tyler/Sofrin-modes and vortex shedding, as well as on the acoustic modes in blade or vane cascades (Parker modes) and cavities is presented. A comprehensive understanding of the underlying physics and the relevant interactions is of vital importance for the safe design of a turbocompressor.

The motivation for the current paper came from studies of impeller failures and extensive research by means of an in-house high-pressure compressor test-stage configuration, which showed that acoustic resonances in the side cavities of the compressor may play a critical role in terms of impeller failures. Some results of the test rig are provided in this paper. Those insights were applied for a root cause analysis of an impeller failure of a five-stage single-shaft compressor for the oil and gas industry. Details on the compressor and the failure pattern will be given in the next section. Aeroacoustic excitation diagrams were derived, which allow the evaluation of critical operating points. The new methodology has been applied to a second impeller failure case, and it seems that this new approach is capable of resolving questions, which were left open previously. This may form a future basis for safe compressor designs.

## CASE HISTORY OF A TYPICAL IMPELLER FAILURE

### *Background Information*

Fortunately, failures on shrouded impellers are quite rare and, even when they happen, they do not necessarily lead to an immediate unit shutdown. Due to the robust rotordynamic design of single-shaft compressors it was experienced several times that, even after loss of some shroud material, operation was continued without interruption. Only after regular inspection of the internals was the damage recognized and tracked down to an earlier point in time, where the shaft vibrations increased somewhat, but stayed below the alarm limit. However, cases are also known, where the impeller damage has hindered free shaft rotation, resulting in a sudden trip.

For application of the methodology outlined in this paper a failure case was selected, which was detected in 2007 on an offshore platform in the Far East. In contrast to cases dated back further, recent cases have the advantage of more complete data being available more easily, as usually comprehensive data are required for a conclusive analysis.

The failed unit being discussed first is a five-stage barrel-type inline compressor for a power of 22.6 MW with a maximum continuous speed of 12,653 rpm. The natural gas with a mole weight of 18.8 is compressed from a design suction pressure of 65.6 bar to a discharge pressure of 160 bar with a temperature rise from 33°C to 120°C. The rated mass flow is 480 000 kg/h.

For the gas export from the platform to an onshore gas plant, two compression trains were installed, each including a gas turbine driving the single-shaft centrifugal compressor through a gearbox. The flow is regulated by the speed of the unit.

### *Failure Description*

After about 22,000 hours of operation accumulated over a period of six years from commissioning one compressor was disassembled. The reason for this inspection was an issue beyond the scope of this paper. After pulling and opening the inner bundle, a fatigue failure on the fifth (last) stage impeller was observed (Figure 1). Three coin-sized pieces broke from the shroud, their locations being about equally spaced around the circumference. The similarity of the deposit layer on all three fracture surfaces with the deposits on the impeller indicates that these fractures must have occurred a significant time before the machine was stopped and opened.


*Figure 1. Fatigue Failure on the Shroud of Stage Five.*

After a certificate review, the failed impeller was subjected to a number of material investigations: visual inspection, nondestructive testing, hardness testing, chemical analysis, and fracture surface investigations using a scanning electron microscope (SEM). For the sake of this paper the result of these comprehensive analyses can be summarized by saying that all properties of the impeller were within specification and that an external excitation mechanism led to a high-cycle fatigue failure. Accordingly, further efforts were related to the derivation of excitation mechanisms, which could conclusively explain this fatigue failure of the shroud.

## EVALUATION OF IMPELLER EXCITATION—A STATE-OF-THE-ART SURVEY

With regard to the state-of-the-art of evaluation of impeller excitation, shrouded centrifugal impellers should be distinguished from semi-open centrifugal impellers and from the airfoils of axial compressor stages. The sensitivity to excitation and the statistical failure frequency is highest for axial blades and lowest for shrouded centrifugal impellers. The available excitation models and analysis tools are directly proportional to this sensitivity.

The complexity of the geometry of shrouded centrifugal impellers, in particular those with a three-dimensional blade surface, mandates application of numerical methods for stress and for modal analysis. The finite element analysis (FEA) is today's standard method. The photorealistic view of the impeller as well as the static-stress distribution in an impeller sector due to the centrifugal load as shown in Figure 2 are derived from such an FEA model.

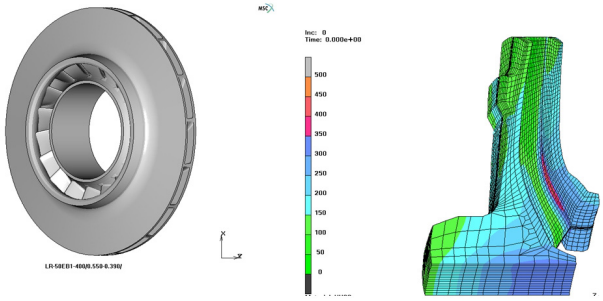

*Figure 2. Photorealistic View and Static-Stress Distribution of an Impeller Sector.*

From the static-stress distribution it is evident that only low static stresses exist at the outer diameter of the shroud. This means in terms of a Goodman or Smith diagram, that relatively high dynamic stresses can be endured in this region of the outer diameter of the shroud, i.e., a strong excitation must prevail there to cause a fatigue failure.

Since high-cycle fatigue always points to high-frequency excitation mechanisms, which might be amplified in a resonance condition with the impeller natural frequencies, a modal analysis is usually conducted. Coincidences of impeller natural frequencies with the frequencies of known forcing functions are checked. The free impeller vibration in a natural frequency is always associated with a certain distribution of the vibration amplitudes, the so-called mode shape. Some examples of such mode shapes are given in Figure 3.

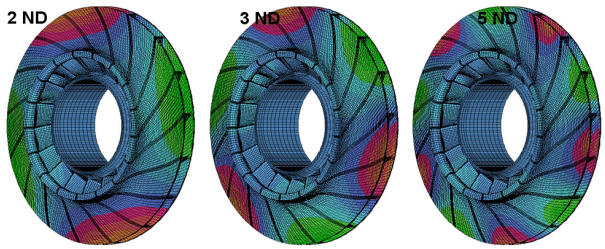


*Figure 3. Mode Shapes with 2, 3, and 5 Nodal Diameters (ND=$m_{struct}$).*

For evaluation of these frequencies and mode shapes it is necessary to categorize the mode shapes according to their number of nodal diameters, nodal circles, and combinations of both. Thereby a nodal diameter or a nodal circle is defined as a line with zero amplitude, defining locations without vibration amplitude. Figure 3 shows examples of the mode shapes with 2, 3, and 5 nodal diameters, while of course also all other nodal diameter modes exist. For the bladed disk of an axial-flow machine the number of nodal diameters can be only as high as half the blade number, for a simple unbladed solid disk the number of nodal diameters is infinite. Shrouded centrifugal impellers lie in-between these extremes and usually also exhibit mode shapes with a higher nodal diameter count than half the blade number.

While the natural frequencies of semi-open centrifugal impeller blades and of airfoils of axial compressor stages are typically presented in a Campbell diagram, it is more meaningful for shrouded centrifugal impellers to categorize the mode shapes by their number of nodal diameters and to generate an interference diagram.

Figure 4 shows such an interference diagram as predicted by FEA for the fifth stage impeller. While the left vertical axis indicates the absolute frequency in Hertz for the predicted natural frequencies, the right vertical axis presents the normalized excitation frequency in terms of harmonics of the rated speed. The blue "zig-zag-line" provides the harmonic order of a forcing function due to rotor/stator interaction with peripheral periodicity, which would match the nodal diameters of the impeller mode shape. At any point in the diagram, where a predicted natural frequency dot is close to this zig-zag-line, a forcing function with the frequency of this harmonic order is matching the impeller mode shape and also its natural frequency, and thus it is theoretically capable of exciting this mode. This needs to be analyzed, of course, for the whole compressor speed range, i.e., the zig-zag line for variable-speed machines is not only a single line, but covers a certain field.

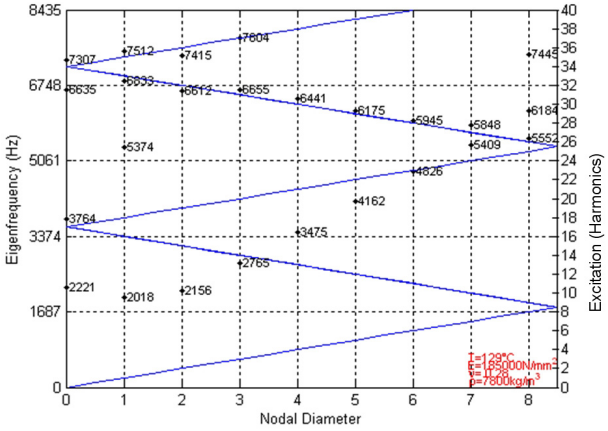


*Figure 4. Interference Diagram of Fifth Stage Impeller.*

This method is usually applied to check whether or not a certain number of stator vanes could excite the impeller to resonant vibrations. In the analyzed case, the compressor has a vaneless diffuser and 22 return vanes. The latter would be capable to excite a 5 ND eigenmode. Figure 4 shows that the 22nd harmonic could come into resonance with a 5 ND mode of the fifth stage at 4162 Hz. While the idea behind this method is certainly correct and represents the current state-of-the-art, it is unfortunately insufficient to explain why impellers fail—or why they don't fail! The proof of this statement can be conducted by analyzing the entire reference basis of centrifugal impellers.

By help of the theory of similitude (all impellers of the original equipment manufacturer [OEM] the authors are working for belong to impeller families, which are geometrically similar) it is possible to predict the natural frequencies of the different mode-shapes for all impellers in service. A database with

normalized modal data has been generated and its validity has been checked with existing results from numerical as well as experimental modal analyses of impellers of different diameter and flow coefficient.

Since the return vanes are of a standard design with a fixed number of vanes (at this OEM), it is possible to derive generically an impeller-tip speed, at which the return vanes excite the impellers of a specific impeller family to resonant vibrations.

Figure 5 shows such a reference chart for the impeller family of the failed fifth stage of the aforementioned case 1 and the second stage of case 2. At a tip speed of u=258 m/s the 5 ND mode of case 2 will be in resonance with 22 vanes. From this chart it is evident that a lot of impellers are operating at this speed in a resonant condition, and only a very few suffered fatigue failure. A further analysis of individual references showed that some of these impellers being operated exactly in resonant condition are in service under quite severe conditions in a most harsh environment (labeled as Specific RESONANT REFERENCES in Figure 5). It must be noted that proper interpretation of this chart should consider the effects of variable-speed drivers as well as of the fact that the line shown at a tip speed of u=258 m/s is an approximation of the exact natural frequency only.

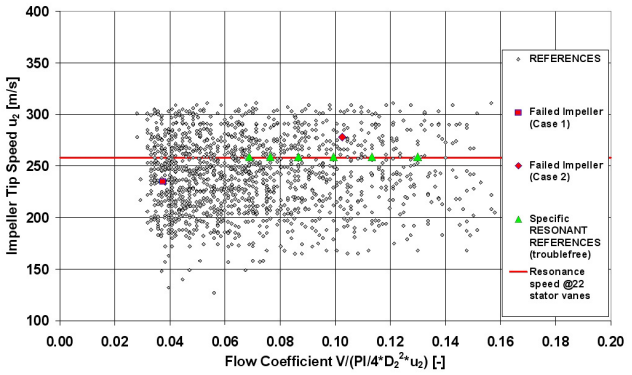


*Figure 5. Reference Chart for 3D Impeller.*

Nevertheless, from the fact of the intersection of the resonance-speed line right through the bulk of reference data, it is concluded that further effects beyond this resonance condition must prevail in order to cause a fatigue failure. Although there are some codes commercially available for prediction of steady-state dynamic impeller stresses, they are unable to predict the interaction of structural modes with further effects such as, for example, acoustic modes within the stage.

## FUNDAMENTALS OF FLOW-INDUCED EXCITATION PHENOMENA

This section gives a short overview on flow-induced excitation mechanisms that are relevant for the aforementioned impeller excitation in centrifugal compressors. Some additional theory is given in APPENDIX A. The well-known phenomena surge and rotating stall are described only briefly (compare APPENDIX A); emphasis is given to phenomena that are less understood with respect to impeller excitation in centrifugal compressors: vortex-shedding and rotor/stator-interaction.

An assessment of the involved interactions within turbomachinery is quite difficult, as can be deduced from Figure 6. The two fields that are commonly treated independently are the fluid and the structure. Though a numerical calculation of fluid/structure interaction (FSI) is possible in principle, it is far from being applicable for realistic turbomachinery applications. The physical mechanism of fluid/structure interaction is as follows: the fluid exerts forces on the confining structure in terms of pressure fluctuations. Those pressure fluctuations lead to vibrations of the rotating or stationary structural components. If the corresponding vibration amplitudes are strong enough, a feedback on the fluid will occur (movement-induced excitation), which leads to a complicated nonlinear coupled system; in this case fluid and structure cannot be treated independently (two-way coupling). A typical example is flutter, a phenomenon classified in the field of aeroelasticity. One example for a two-way coupling between fluid and structure in centrifugal turbomachinery can be found in Eckert (1999). They delivered a root cause of an impeller failure of a radial fan based on an aeroelastic excitation mechanism: the acoustic field in the fan side room led to impeller vibrations, which in turn led to variations of the leakage flow rate due to variations of the seal gap width. The acoustic field itself was mainly excited by the variation in leakage flow. This feedback loop resulted in strong vibration amplitudes of the fan impeller.

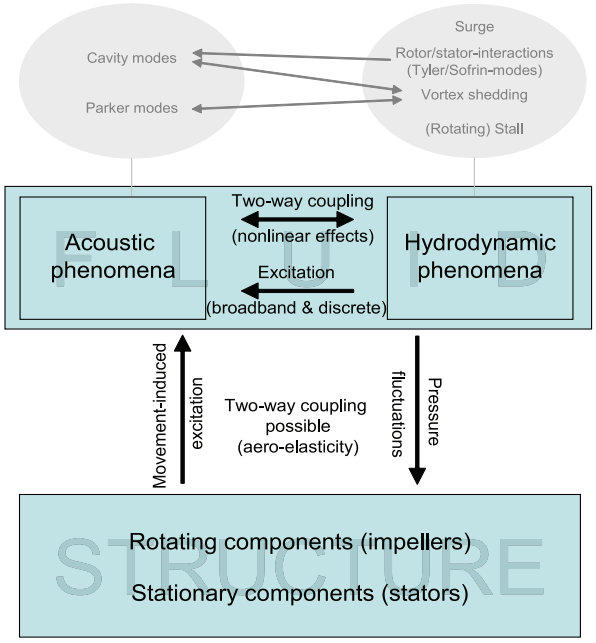


*Figure 6. Fluid/Structure Interaction Mechanisms.*

Even if the two-way coupling mentioned above is not taken into account, the fluid alone can exert forces on the structure that are strong enough to lead to structural failures. The characteristics of the fluid can be subdivided into two categories that are allocated as acoustic (associated with the compressibility of the fluid) and purely hydrodynamic (compare Figure 6). Hydrodynamic oscillations may be broadband or may exhibit discrete frequencies due to periodic events. Both types of hydrodynamic fluctuations may excite acoustic eigenmodes, leading to resonance conditions. If, due to such a resonance condition, the acoustic fluctuations exceed a certain limit, the classic approach of linear acoustics is no longer valid. In such cases, the acoustic modes cannot be decoupled from the vorticity and entropic modes of the fluid and the whole fluid system is fully coupled (two-way coupling).

In Figure 6 several distinct phenomena are allocated to the acoustic and hydrodynamic fields. These may interact, visualized in terms of arrows that indicate the interactions as “one-way” or “two-way.” The separate phenomena are discussed in the following sections and in APPENDIX A. For the analysis purposes discussed in the current paper, the acoustics, fluid dynamics, and mechanics are treated separately. This simplification is necessary, since the aim of the current study is the development of a methodology that is applicable in an industrial context.

### *Vortex-Shedding*

The interest in vortex-shedding for turbomachinery applications originates from the fact that this phenomenon may lead to an aeroacoustic coupling inside the machine. Such a coupling will in

turn lead to amplified vortex-shedding amplitudes that may result in structural failure. In general, under the influence of flow, any bluff body and any cavity will shed vortices. Bluff bodies typical for turbomachinery are instrument probes, heat exchangers, and struts. The latter may be stationary (vanes) or rotating (blades). Cavities, the second category, are omnipresent in turbomachinery, and the vortex-shedding mechanism originates from the inherent instability of the shear layer at the cavity edges. A detailed description of many vortex-shedding mechanisms relevant in turbomachinery can be found in Lucas, et al. (1997).

In general, the frequencies due to vortex-shedding can be estimated if a nondimensional Strouhal number is introduced:

$$\mathrm{St} = \frac{fL}{c}. \tag{1}$$

The Strouhal number relates a characteristic length $L$, the vortex shedding frequency $f$, and the flow velocity $c$. For practical applications, the definition of representative Strouhal numbers, realistic geometry parameters, and flow velocities is far from being straightforward. A detailed discussion on this topic can be found in APPENDIX A.

*Rotor/Stator-Interactions*

It can be shown that rotor/stator interaction produces a plurality of spinning modes corresponding to a single frequency. The theoretical basis of the generating mechanism was first presented in the famous paper of Tyler and Sofrin (1961). With respect to this fundamental work the modes generated by rotor/stator interaction are nowadays commonly referred to as *Tyler/Sofrin modes*.

The spectrum of the noise due to a rotor interacting with a nonuniform steady flow (e.g., the potential field of a stator) is discrete with spectral lines at the blade-passing frequency and harmonics. The corresponding interaction field for a particular harmonic, $h_B$, of blade-passing frequency, is a superposition of an infinite number of rotating patterns. The number of circumferential lobes in each pattern is given by the circumferential mode order $m_{TS}$, which, perfect periodicity assumed, follows the expression:

$$m_{TS} = h_B z_B + h_V z_V. \tag{2}$$

$z_B$ denotes the number of rotating impeller blades, the index $h_V$ ranges over all positive and negative integers, and $z_V$ indicates the number of stationary vanes. This amounts to adding and subtracting multiples of the number of vanes from the product $h_B \bullet z_B$. Each resulting $m_{TS}$-lobe pattern turns at a different circumferential phase speed in the stationary frame of reference. This speed is commonly much higher than the rotor-shaft speed $\omega^S_{shaft}$ and can even become supersonic:

$$\omega^S_{ph,TS} = \frac{h_B z_B}{m_{TS}} \omega^S_{shaft}. \tag{3}$$

Positive values of $m_{TS}$ indicate modes spinning in the rotor's sense of rotation (positive $\omega^S_{ph,TS}$), whereas negative $m_{TS}$ indicate modes counterrotating with respect to the rotor's sense of rotation (negative $\omega^S_{ph,TS}$).

When a rotating-pressure pattern of mode order $m_{TS}$ and frequency $\omega^S_{TS}$ (the superscript S indicates the stationary frame of reference) interacts with a stator having $z_{V2}$ vanes, additional modes:

$$\omega^{S\,*}_{TS} = \omega^S_{TS}, \tag{4}$$

$$m^*_{TS} = m_{TS} + h_{V_2} z_{V_2}, \quad h_{V_2} = \ldots, -2, -1, 0, 1, 2, \ldots \tag{5}$$

$$\omega^{S\,*}_{ph,TS} = \frac{\omega^{S\,*}_{TS}}{m^*_{TS}} \tag{6}$$

are generated. In the rotating frame of reference the frequencies resulting from the interaction between a rotating blade row and two stationary vane rows can be derived from:

$$\begin{aligned} \omega^{R\,*}_{TS} &= \left|(\omega^{S\,*}_{ph,TS} - \omega^S_{shaft}) \cdot m^*_{TS}\right| = \left|\omega^{S\,*}_{TS} - \omega^S_{shaft} \cdot m^*_{TS}\right| = \left|h_B z_B - m^*_{TS}\right| \cdot \omega^S_{shaft} \\ &= \left|h_{V_1} z_{V_1} + h_{V_2} z_{V_2}\right| \cdot \omega^S_{shaft} \end{aligned} \tag{7}$$

To avoid the concept of negative frequencies only absolute values are considered.

One example where the generation of such "secondary" modes was verified can be found in Kennepohl, et al. (2001). In principle, many of these interactions are possible. If one rotor (or several rotors with the same blade count and the same rotor speed) interacts with a number of vane rows, the above considerations lead to the following formula for the circumferential mode orders:

$$m_{TS} = h_B z_B + \sum_{i=1}^{N_V} h_{V_i} z_{V_i}, \tag{8}$$

where $N_V$ denotes the number of vane arrays. In analogy to the derivation in Equation (7) these Tyler/Sofrin-modes are characterized by the following frequencies in the rotating frame of the impeller ($\omega^S_{shaft}$ indicates the shaft angular frequency in the stationary frame of reference):

$$\omega^R_{TS} = \omega^S_{shaft} \cdot \left|\sum_{i=1}^{N_V} h_{V_i} z_{V_i}\right| \tag{9}$$

In the stationary frame of reference these frequencies correspond to the blade-passing frequency and harmonics.

Since the generation of Tyler/Sofrin-modes due to rotor/stator interaction is unavoidable in practical applications a profound knowledge of the underlying physics is necessary to avoid a possible influence on machine failures.

## ACOUSTIC RESONANCES IN CENTRIFUGAL COMPRESSORS

Acoustic resonances may lead to strong pressure fluctuations of confined fluid domains, leading to noise and, in the worst case, to structural failure. Due to the large number of cavities and the inherently unsteady flow field in turbomachinery, those machines are especially sensitive to such resonances. The more-or-less confined turbomachinery cavities exhibit characteristic eigenfrequencies, and the complex flow field constitutes a large variety of strong excitation sources. Different mechanisms may act as excitation sources, such as vortex-shedding and Tyler/Sofrin-modes. If the excitation frequency approaches one of the acoustic eigenfrequencies, care and a profound understanding of the interaction mechanisms is necessary to evaluate the relevance of such a condition. In general, a frequency coincidence alone is not considered critical; moreover, a correlation between the shape of the excitation pattern and the acoustic mode must exist (e.g., in terms of the same number of nodal diameters). The stronger this correlation, the stronger the expected pressure fluctuations. In terms of their excitation pattern and frequency Tyler/Sofrin-modes are well defined: in the stationary frame of reference they are characterized by the blade-passing frequency and harmonics, and the number of nodal diameters can be easily calculated from the blade and vane counts of the relevant components. Vortex-shedding, on the other hand, can neither be easily attributed to a certain frequency (due to the uncertainties in Strouhal number), nor to a distinct pressure pattern. In any case, the first step to evaluate possible acoustic resonance conditions is the calculation of the acoustic eigenfrequencies of the relevant cavities. In APPENDIX A this is presented as an example for two typical acoustic phenomena in turbomachinery: the acoustic modes in the side cavities of centrifugal compressors and the acoustic modes that are localized to blade or vane arrays.

## TEST RIG FOR STUDIES OF EXCITATION PHENOMENA IN CENTRIFUGAL COMPRESSORS

To study excitation mechanisms in centrifugal compressors an in-house test rig has been established. Several years of development time were necessary for preliminary studies, design, manufacturing,

and assembly of the test rig, as well as establishing and validating the required measurement techniques. Lots of experimental data have been collected so far, and much more will follow. A presentation of all relevant insights would fill several papers and is well beyond the scope of the overview paper at hand. A first selection of results has already been published by Petry, et al. (2009), and some additional results will be given in this paper.

*Test-Rig and Experimental Setup*

The test rig represents a typical stage of a high-pressure single-shaft compressor, including inlet guide vanes (IGV), a typical high-pressure shrouded 2D-impeller, a vaned low-solidity diffuser (LSD), and a return guide vane (RGV) cascade. A picture of the test rig internals is given in Figure 7. The test rig parameters are presented in Table 1. A sectional drawing of the compressor is given in Figure 8. The compressor is operated in closed loop and can be operated at variable speeds.

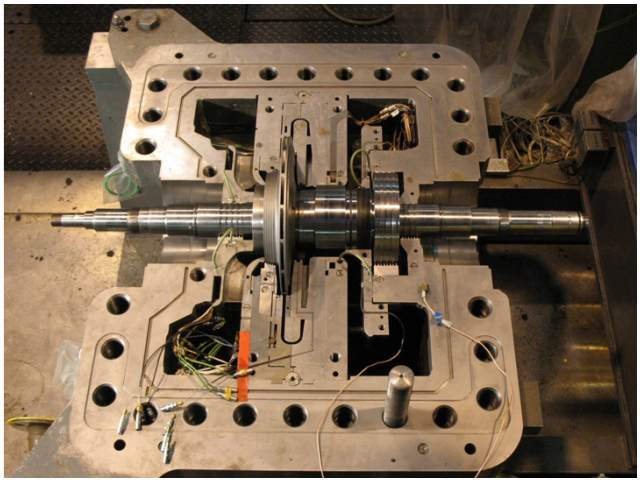

*Figure 7. Picture of Test Rig.*

*Table 1. Test Rig Parameters.*

| | |
|---|---|
| Flow coefficient, $\varphi$ | 0.0106 |
| Number of impeller blades, $B$ | 17 |
| Number of diffuser vanes, $z_{Dif}$ | 10 |
| Number of inlet guide vanes, $z_{IGV}$ | 18 |
| Number of return guide vanes, $z_{RGV}$ | 22 |
| Impeller outer diameter, $D_2$ | 350 mm (1.15 ft) |
| Hub-to-tip ratio, $D_1/D_2$ | 0.425 |
| Max. speed of rotation, $n_{max}$ | 15900 rpm |
| Max. circumferential velocity, $u_{2,max}$ | 292 m/s (958 fps) |

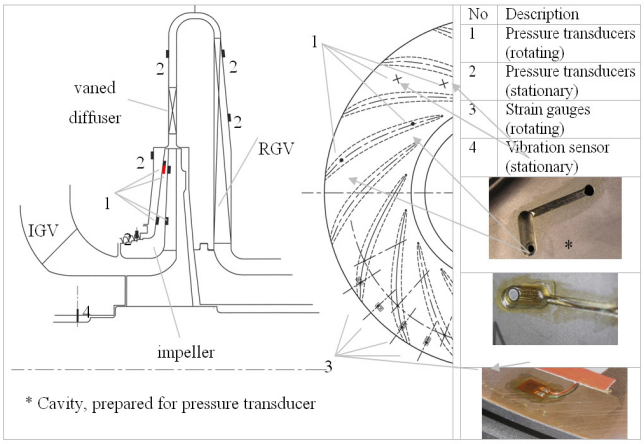


*Figure 8. Test Rig and Instrumentation.*

*Measurement Techniques*

To detect the different possible excitation mechanisms and the vibrations of the impeller disk, the test rig is equipped with a multiplicity of dynamic (temporal high resolution) pressure transducers, strain gauges, and vibration transducers on the stationary side (compressor housing), as well as on the rotating side (cover disk of the impeller). A detailed description of the measurement techniques can be found in Petry, et al. (2009).

Of special interest for the current paper is the piezoresistive miniature pressure transducer with the red label in Figure 8. This transducer is located on the impeller shroud disk (rotating frame of reference) at $0.92 \bullet D_2$.

## TRANSIENT CFD ANALYSIS OF TEST-STAGE CONFIGURATION

To gain a better understanding of the relevant rotor/stator-interaction mechanisms a transient CFD calculation of the whole test-stage configuration as depicted in Figure 8 was carried out. A commercial CFD code was used for a transient full-3D analysis including all blade and vane rows (inlet guide vanes, rotor blades, LSD vanes, and return guide vanes). The numerical setup was optimized in such a way that the relevant rotor/stator-interaction mechanisms could be covered within a reasonable timeframe from a research point of view. Nevertheless, several weeks of calculation time on four parallel CPUs with 2.6 GHz and 2GB RAM each were necessary to obtain a converged solution. The transient simulation covered 12 impeller revolutions and a time-step representing one degree of rotation was chosen in order to provide a good resolution of the dynamic pressure pattern for one revolution. More details on the numerical modeling can be found in Petry, et al. (2009).

As already mentioned, one main focus of the current investigation is phenomena associated with rotor/stator-interaction. To the authors' knowledge, up to now, no systematic studies were available that cover the generation of rotating pressure patterns due to the interaction between rotating and stationary components in centrifugal compressors. The current simulation gives insight into those phenomena. In Figure 9 the instantaneous distribution of such a pressure pattern is shown. It can be seen that the hub disk of the rotor experiences a strong pressure fluctuation with seven lobes on the circumference. The pressure maxima are located at the impeller outer radius and it strikes one's eye that a certain correlation with typical mechanical eigenmodes exists (compare Figure 3). For the shroud disk the seven lobes pattern is also dominant, but not as obvious as for the hub disk. In the current case, a resonance condition would occur if the seventh nodal diameter structural eigenfrequency of the impeller coincided with the frequency of the depicted Tyler/Sofrin mode (coincidence between mode shape and frequency). If an

additional coincidence (frequency and mode shape) with an acoustic eigenmode in the side cavities would occur, the resonance condition would be much more severe. However, for the given operating point, no resonance conditions are expected for the seventh nodal diameter mode. In this context, it is worth mentioning that a CFD calculation is capable of simulating a resonance condition between Tyler/Sofrin-modes and acoustic eigenfrequency from a physics point of view, since the Helmholtz equation follows from the governing equations of fluid mechanics. However, higher-order numerical schemes are mandatory to resolve such effects, and even then, great care is necessary to correctly resolve the acoustic behavior of the fluid. Of course, a resonance condition with the structure can only be calculated by means of a coupled fluid-structure interaction simulation. Considering the computational effort for the CFD calculation alone, such an FSI analysis is far from being feasible for the current configuration.

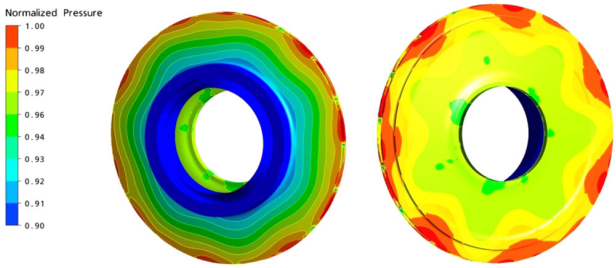


*Figure 9. Instantaneous Pressure Distribution on Impeller (Left: Shroud Side, Right: Hub Side).*

More information on the modal structure of the pressure field is given as an example for the circumference of the radial position of the stationary pressure transducer in the shroud-side cavity (at $0.97 \bullet D_2$, compare Figure 8). Since the pressure fluctuations at the blade-passing frequency and harmonics are a superposition of many spinning modes with different circumferential mode order, an experimental modal analysis of the underlying pressure field is almost impossible: to resolve a pattern with $m$ lobes on the circumference $2 \bullet m$ sensors would be required. Given the space constraints within the test rig it becomes clear that an experimental modal analysis is not feasible. The transient CFD results, on the other hand, constitute a valuable database for such an evaluation: For a numerical modal analysis a fast Fourier transform (FFT) of the instantaneous pressure distribution for one given time-step and one radial position is carried out. According to the FFT methodology this pressure distribution is decomposed into sine-waves of harmonic order $m$ with corresponding amplitudes and phase angles. The resulting amplitudes for each mode order up to $m$=55 are given in Figure 10 (left) for the radial position $0.97 \bullet D_2$. The FFT spectrum clearly reveals that indeed the mode with seven lobes on the circumference ($m_{TS}$=7) is dominant. This mode, in the stationary frame of reference, is rotating with a circumferential phase velocity of 17/7 times rotor speed, which is in agreement with Equation (3). This phase velocity must be multiplied by the mode order to obtain the frequency that a stationary observer would experience. For all Tyler/Sofrin modes that result from the interaction with the rotor blades fundamental ($h_B$=1 in Equation [2]), this is the blade-passing frequency. In other words: the peak at the blade-passing frequency in the FFT spectrum (compare Figure 10 [right]) corresponds to a superposition of a large variety of Tyler/Sofrin modes, which are characterized by $h_B$=1 in Equation (2). For all Tyler/Sofrin modes with $h_B$=2 (the first rotor harmonic) two times the blade-passing frequency will be observed, and so on. In Figure 10 (right), it can be seen that, as expected, the harmonics of the blade-passing frequency are much weaker than the fundamental.

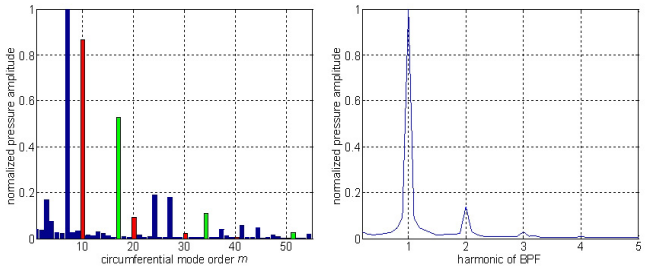


*Figure 10. Modal Analysis (Left) and Frequency Analysis (Right) from CFD Calculation.*

In Figure 10, besides the dominant $m_{TS}$=7 mode, there is a large variety of additional modes. The pressure patterns that result from the potential field of the LSD vanes alone (located downstream of the measurement position) are labeled in red. According to Equation (2), those are the modes with $h_B$=0 (no rotor/stator-interaction). The corresponding pressure fields are stationary in the absolute frame of reference (which is in agreement with Equation [3]), and, in the rotating frame of reference, are observed as harmonics ($h_V$ in Equation [2]) of the vane-passing frequency. It can be seen that the fundamental of the 10 LSD vanes constitutes the second strongest component in the spectrum, but the harmonics decay rapidly. Similarly, the pressure patterns that result from the impeller blades alone are labeled in green. Those modes are characterized by $h_V$=0 in Equation (2), and, if multiplied with the mode order $m_{TS}$ in Equation (3), are observed as the blade-passing frequency and harmonics in the stationary frame of reference. Of course, in a frame of reference rotating with the impeller, those modes are stationary. In Figure 10 the "rotor-alone" modes are characterized by the number of impeller blades (17) and harmonics. It is interesting to note, that, at the measurement position in the shroud-side cavity, the $m_{TS}$=17 pressure pattern due to the rotor blades alone is weaker than the $m_{TS}$=10 pressure field due to the LSD vanes alone. However, higher harmonics decay more rapidly for the LSD vanes.

Besides the "rotor-alone" and "LSD-alone" modes many additional modes exist (labeled in blue in the mode spectrum in Figure 10 [left]). These are the modes due to rotor/stator-interaction according to Equation (2). As already mentioned, those modes are characterized by the blade-passing frequency and harmonics $h_B$ in the stationary frame of reference, and the vane-passing frequency and harmonics $h_V$ in the rotating frame of reference. All peaks in the spectrum can be attributed to rotor/stator-interaction. The modes with the strongest relative amplitudes are given in Table 2. As already discussed, by far the strongest pressure pattern results from the fundamental interaction between impeller blades and LSD vanes ($m_{TS}$=7). Furthermore, it is interesting to note that the modes with negative $h_V$ (smaller values of $m_{TS}$) experience stronger amplitudes than the modes with positive $h_V$. Rotor harmonics lead to stronger amplitudes than the respective LSD harmonics (compare $24=2 \bullet 17-1 \bullet 10$ and $-3=1 \bullet 17-2 \bullet 10$). This observation is in agreement with strength of the "rotor-alone" and the "LSD-alone" modes. The latter are weaker for harmonics of the same order.

Two modes in Table 2 that cannot be explained by the interaction between impeller blades and LSD vanes are $m_{TS}=-1$ and $m_{TS}=-2$. Those modes are a result of the interaction between the 17 impeller blades and the 18 inlet guide vanes. As for the impeller/LSD interaction, the fundamental Tyler/Sofrin mode is stronger than the "IGV-alone" mode with 18 lobes on the circumference.

It has to be mentioned that no interaction between impeller blades and return guide vanes could be resolved from the CFD analysis. This is not consistent with the experimental results, where this interaction was found to be surprisingly strong (compare Petry, et al., 2009). Further studies are necessary to understand this phenomenon.

*Table 2. Tyler/Sofrin Modes from CFD Calculation.*

| $m_{TS}$ | $h_B$ | $h_V$ | amplitude |
|---|---|---|---|
| 7 | 1 | -1 | 1 |
| 24 | 2 | -1 | 0.19 |
| 27 | 1 | 1 | 0.18 |
| -3 | 1 | -2 | 0.17 |
| 4 | 2 | -3 | 0.076 |
| 41 | 3 | -1 | 0.057 |
| 44 | 2 | 1 | 0.046 |
| -1 | 1 | $h_{IGV}$=-1 | 0.040 |
| 37 | 1 | 2 | 0.039 |
| -2 | 2 | $h_{IGV}$=-2 | 0.035 |

## AEROACOUSTIC EXCITATION MODEL FOR SIDE CAVITIES OF CENTRIFUGAL COMPRESSORS

Based on the theory presented in the preceding sections and new insights from basic experimental and numerical investigations, an aeroacoustic impeller-excitation evaluation procedure has been developed. The underlying methodology can be visualized in an evident diagrammatical form for each circumferential mode order. The diagrams visualize the interaction mechanisms between acoustic eigenmodes in the centrifugal compressor side cavities, the corresponding impeller structural mode shape, and the corresponding excitation due to Tyler/Sofrin modes.

Due to an improved understanding of the relevant mechanisms, the development of those diagrams has undergone several improvements over the last months. The starting point was a simple two-dimensional acoustic model of the side cavities, and today, full-3D finite element acoustic analyses of the whole compressor stage are included. Both approaches are useful; the simple one for a first estimate, and the more advanced one for a detailed analysis. The latest improvement of the excitation analysis methodology is based on experimental results that were obtained only recently: the inclusion of the influence of swirling flow in the side cavities. All those aspects will be discussed in the following subsections.

### *Two-Dimensional Analytical Side Cavity Model*

For annular ducts with rigid walls the procedure to calculate the acoustic eigenmodes is well known and can be found in many textbooks. If inlet and outlet of the duct are confined by solid walls, the reflections at the boundaries can lead to standing waves in the axial direction. This is the case for confined annular cavities. Mathematically this can be expressed as follows (see for example Ehrich, 1969):

$$\omega^{S}_{ac_{mnj}} = a\left[\left(\frac{s_{mn}}{R_2}\right)^2 (1-M_{ax}^2) + \left(\frac{j\pi(1-M_{ax}^2)}{l_{ax}}\right)^2\right]^{1/2} + m_{ac}\omega^{S}_{swirl} \quad (10)$$

$\omega^{S}_{ac} \equiv \omega^{S}_{acmnj}$ corresponds to the eigenfrequency of a cavity eigenmode in the stationary frame of reference with $m \equiv m_{ac}$ diametral nodes, $n \equiv n_{ac}$ node circles, and $j \equiv j_{ac}$ axial nodes. $m_{ac}$ may take positive and negative values, the latter indicating modes spinning in the opposite direction of the rotor sense of rotation (with respect to the reference system of the rotating acoustic mode). $a$ denotes the speed of sound, which is assumed constant in the fluid medium. $M_{ax}$ is the constant axial Mach number, and $l_{ax}$ the axial length of the chamber. $s_{mn}$ are the roots of a characteristic equation. In Ehrich (1969) this equation is given for rigid wall boundary conditions at the inner and outer radius. However, for a chamber representing a side cavity of a centrifugal compressor, the boundary condition at the outer radius $R_2$ is better approximated by an acoustical soft wall boundary condition (pressure node), compare König (2009).

One important parameter for centrifugal compressors is the fluid rotation in the side cavities. In Equation (10) this influence is included with the summand $m_{ac}\omega^{S}_{swirl}$, whereby $\omega^{S}_{swirl}$ is the solid-body swirl angular velocity of the fluid in the side cavity (note that in Ehrich (1969) this quantity is associated with the swirl in axial turbomachines). This influence may be thought of as a transformation from the rotating frame of reference of the fluid core to the stationary frame of reference. Usually it is a good guess to assume that the core rotates with half the circumferential speed $\omega^{S}_{shaft}$ of the rotor (compare, e.g., Schlichting, 1965), which means $\omega^{S}_{swirl} = 0.5 \cdot \omega^{S}_{shaft}$. All studies known to the authors neglect this influence; however, this will result in large deviations, especially for high mode orders $m_{ac}$ and high rotational speeds. The necessity of the inclusion of this swirl correction will be shown in the next but one subsection.

In reality, the flow field and geometry of the side cavities of a centrifugal compressor are much more complex than the analytical model described above. However, the application to several compressors revealed that in some cases the accuracy of the simple two-dimensional model is completely sufficient. Some aspects that cannot be covered by simple analytical means are discussed in the following subsection.

### *Three-Dimensional Finite-Element Side-Cavity Model*

The analytical approach fails as soon as the cavity-surrounding geometry deviates strongly from the model of a two-dimensional annular cavity. For high-pressure centrifugal compressors with 2D-blading those deviations are usually quite small; for 3D-blading, however, an accurate modeling of the side cavity geometry is recommended.

Besides the purely geometrically induced uncertainties, a 3D analysis is capable of resolving mode-coupling mechanisms with connecting cavities. Such coupling mechanisms may lead to eigenfrequencies of the coupled mode well away from the eigenfrequencies of the local side-cavity modes. Furthermore, the finite element method allows the consideration of spatially varying speed of sound and density fields. Those aspects are discussed in detail in König (2009).

Even with the finite element method the influence of the complex transient flow field on the acoustic eigenfrequencies cannot be accounted for. However, in analogy to the two-dimensional model, the analytical swirl correction can be applied to the calculated eigenfrequencies to include the influence of the rotating fluid in the side cavities. This step is necessary, as will be shown in the next subsection.

### *Influence of Swirling Flow in the Side Cavities*

It is common practice to think of the fluid in the side cavities of centrifugal turbomachinery as a rigid body rotation (imagine a rotating disk) with a constant circumferential velocity. However, in reality, due to the boundary layers and through-flow of the cavities, this is only a crude approximation. As already mentioned, it is

usually assumed that the fluid core angular velocity is half the circumferential speed of the rotor ("swirl factor" of 0.5). In Figure 11 the swirl factor in the side cavities from the transient simulation of the test-stage configuration (refer to Figure 8) is given for one representative time-step. It can be seen that for this configuration a swirl factor of 0.5 constitutes a reasonable average, but distinct deviations from this constant value are obvious. It is interesting to note that the swirl factor in the hub-side cavity is lower than the swirl factor in the shroud-side cavity. Though it has to be mentioned that the grid resolution of the CFD mesh at hand is too coarse to capture the correct boundary layer characteristics, it is assumed that the results give a reasonable indication of the general behavior.

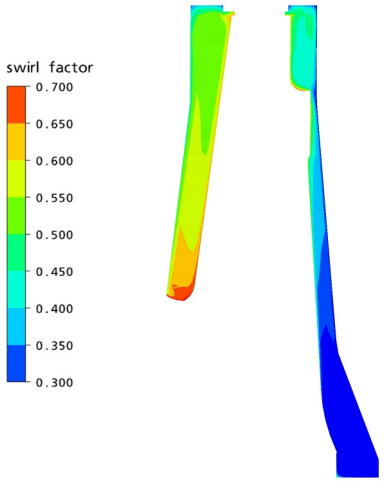


*Figure 11. Swirl Factor from CFD Calculation.*

*Mathematical Background*

When talking about acoustic modes in the side cavities of centrifugal compressors, as already mentioned, the fluid rotation has to be taken into account. If the model of a fluid rigid-body rotation is adopted (the fluid rotates with $\omega^{S}_{swirl}$), the rotating fluid core constitutes the reference system of the acoustic mode. Within this acoustic reference system the acoustic mode is characterized by its eigenfrequency $\omega^{A}_{ac}$. This is the frequency that an observer rotating with the swirling fluid core would experience. In this rotating frame of reference the acoustic mode may be thought of as a spinning pressure-pattern rotating with the phase velocity:

$$\omega^{A}_{ph,ac} = \omega^{A}_{ac} / m_{ac} \tag{11}$$

For positive $m_{ac}$ the mode is rotating in the positive direction with respect to the reference system of the acoustic mode, while for negative $m_{ac}$ it is counterrotating, respectively. Accordingly, a standing fluctuating pressure-pattern will be observed in the reference system of the acoustic mode if two modes with opposite sign of $m_{ac}$ are superimposed.

In the stationary system, the circumferential phase velocity of the acoustic mode is given by:

$$\omega^{S}_{ph,ac} = \omega^{A}_{ph,ac} + \omega^{S}_{swirl} \tag{12}$$

The transformation into the relative frame of the rotor leads to:

$$\omega^{R}_{ph,ac} = \omega^{A}_{ph,ac} + \omega^{S}_{swirl} - \omega^{S}_{shaft} \tag{13}$$

To obtain the relevant frequencies the circumferential phase velocities must be multiplied by their corresponding circumferential mode order. One obtains:

$$\omega^{S}_{ac} = \omega^{A}_{ac} + m_{ac} \cdot \omega^{S}_{swirl} \tag{14}$$

$$\omega^{R}_{ac} = \omega^{A}_{ac} + m_{ac} \cdot \left(\omega^{S}_{swirl} - \omega^{S}_{shaft}\right) \tag{15}$$

*Experimental Verification*

The above formulae were derived in a purely mathematical sense and in that respect are completely plausible. However, the application of this idea cannot be found in open literature and no supporting experimental evidence is openly available. Since such data are urgently needed for model validation purposes, unsteady pressure measurements obtained from the test rig depicted in Figure 8 have been analyzed with respect to the occurrence of acoustic resonances in the side cavities. In Figure 12 and Figure 13 the normalized pressure signals for a run up from 5000 rpm to 15,000 rpm for two different rotor harmonic speed lines are depicted. A detailed description of the data analysis procedure would be beyond the scope of this paper but can be found in Petry, et al. (2009). The unsteady pressure signals were obtained in the rotating frame of reference with the red-labeled sensor in Figure 8. In Figure 12 the 52nd and in Figure 13 the 62nd rotor-harmonic speed lines are plotted. In each pressure trace a distinct peak occurs that can be attributed to an acoustic resonance in the side cavity. In Figure 12 this frequency corresponds to an acoustic mode with 18 lobes on the circumference and in Figure 13 to a mode with 28 lobes on the circumference. The calculation of both acoustic modes was carried out by means of 3D finite element tools and it was found that both modes are coupled between hub and shroud-side cavity. As an example, the calculated pressure-amplitude distribution for $|m_{ac}|$=18 on the impeller shroud disk is given in Figure 14. Clearly, the mode shape can be identified (36 red pressure-amplitude regions according to 18 nodal diameters). For a comparison with the experiment two parameters must be estimated that are affected by a certain degree of uncertainty: a representative speed of sound (that is a realistic mean temperature) and a representative swirl factor. On the basis of Figure 11 and values found in literature the swirl factor was set to 0.5, and the representative temperature was estimated by in-house design tools. Excellent agreement between the predicted acoustic eigenfrequencies and the measured resonance frequencies was found: the deviations between frequency prediction and the experimentally determined resonance peaks amount to values as low as 0.8 percent for the $|m_{ac}|$=18 case, and 2.2 percent for the $|m_{ac}|$=28 case, respectively.

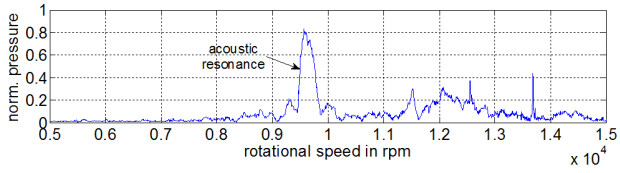


*Figure 12. Runup for 52nd Rotor Speed Harmonic (Rotor Frame of Reference).*

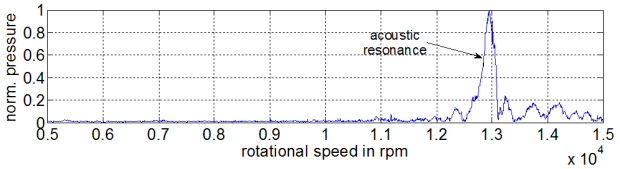


*Figure 13. Runup for 62nd Rotor Speed Harmonic (Rotor Frame of Reference).*

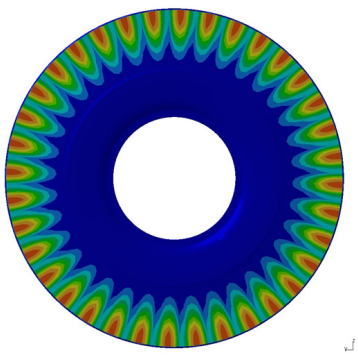

*Figure 14. Pressure Amplitude Distribution for $|m_{ac}|$=18.*

Those are only two examples where agreement between calculated and measured acoustic eigenfrequencies could be found *if the swirl correction was applied*. Without swirl correction none of the peaks in the pressure traces could be clearly attributed to an acoustic resonance. Those results show that a swirl correction is absolutely mandatory to evaluate the acoustic behavior in the side cavities. If neglected, very large deviations from the calculated eigenfrequencies may occur.

At the current stage no measured temperature values are available. For further model improvement, subsequent experiments will include temperature measurements in both side cavities. With this information, uncertainties in the calculated speed of sound can be minimized and a model calibration by means of a representative swirl factor can be carried out.

It is worth mentioning that mainly acoustic resonances with high circumferential mode order could be identified in the pressure signals. For lower mode orders, which occur at much lower frequencies, the disturbances from the hydrodynamic pressure fluctuations complicate the data analysis. Future studies will focus on the absolute amplitudes of the pressure fluctuations as a function of their mode order and on their potential to lead to impeller failures.

Up to now, nothing has been said on the excitation mechanism leading to the resonance peaks in Figure 12 and Figure 13. From a detailed analysis of the experimental data it was found that all peaks in the pressure signal that are attributed to acoustic resonances in the side cavities occur at frequencies that are multiples of the rotor speed. In Figure 12 this is the 52nd rotor speed harmonic, and in Figure 13 the 62nd. All those harmonics can be clearly attributed to the interaction between rotor blades and stator vanes. The two examples given in the current paper are characterized by the interaction between the second rotor-blade harmonic and higher harmonics of the stator vane arrays, whereupon two respective interaction scenarios are plausible (compare Table 3 and Table 4 in combination with Equation [8]). Surprisingly, all those interactions are based on secondary Tyler/Sofrin modes (compare Petry, et al., 2009). Based on these interactions the sign of the acoustic mode orders can be determined, which is negative for both examples.

*Table 3. Rotor/Stator Interactions Leading to m=−18.*

| $h_B$ | $h_{LSD}$ | $h_{RGV}$ | $h_{IGV}$ |
|---|---|---|---|
| 2 | -3 | -1 | 0 |
| 2 | 1 | -2 | -1 |

*Table 4. Rotor/Stator Interactions Leading to m=−28.*

| $h_B$ | $h_{LSD}$ | $h_{RGV}$ | $h_{IGV}$ |
|---|---|---|---|
| 2 | -4 | -1 | 0 |
| 2 | 0 | -2 | -1 |

Two important conclusions can be drawn from the experimental findings: First, acoustic modes in the side cavities can be excited by Tyler/Sofrin modes. This hypothesis is included in the excitation model presented later. Second, higher harmonics of the rotor and stator vane arrays may lead to acoustic resonance conditions, and even vane arrays located far downstream are relevant! The second finding was quite surprising and will be investigated in more detail in the future. Information is urgently needed in how far those secondary interactions may lead to critical impeller excitation. Neither conclusion has ever been reported in open literature but may have a strong impact on future designs. They clearly show that basic experimental studies are essential to further improve such complicated systems as turbomachinery.

*Acoustic Harmonic Excitation Analysis Diagram (AHEAD)*

Many new insights could be derived from the numerical and experimental investigations presented in the preceding sections. For practical application purposes, based on the new findings, a methodology had to be established to allow straightforward evaluation of critical compressor operating points. For this reason the *acoustic* eigenfrequencies, the *harmonic excitation* due to Tyler/Sofrin modes, and the impeller eigenfrequencies are analyzed graphically in the so-called acoustic harmonic excitation analysis diagram (AHEAD).

The underlying principle of AHEAD is visualized in Figure 15. Two prerequisites are necessary for a strong coupling between acoustic mode and structural mode to occur: first, in the same frame of reference, the eigenfrequencies of both modes must coincide (at least they must be close to each other). Second, the number of nodal diameters must be the equal for both modes. The strength of the coupling then depends on the radial distribution of the mode shapes. This "coupling of modes" is illustrated in the rectangle in Figure 15. In this example both modes are characterized by five nodal diameters ($|m_{ac}|=|m_{struct}|=5$). For a critical operating condition to occur, the acoustic mode must be excited by a forcing function. It was shown in the preceding sections that one relevant excitation source constitutes the Tyler/Sofrin modes resulting from rotor/stator interaction. Those modes are characterized by well-defined frequencies and mode shapes. As for the coupling between acoustic and structural modes, a coupling between Tyler/Sofrin modes and acoustic eigenmodes occurs if the respective circumferential mode orders and frequencies coincide. Mathematically a critical coupling between Tyler/Sofrin mode, acoustic eigenmode, and structural eigenmode is defined as follows:

$$m_{TS} = m_{ac} = m_{struct} \tag{16}$$

$$\omega^R_{TS} \approx \omega^R_{ac} \approx \omega^R_{struct} \tag{17}$$

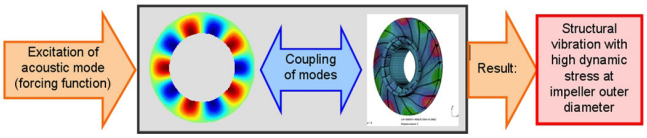


*Figure 15. Basic Principle of Mode-Coupling Mechanism.*

Operating conditions that lead to such a triple coupling are considered critical with respect to possible impeller failures. Besides Tyler/Sofrin modes, vortex-shedding may also trigger an acoustic resonance. The respective frequencies are also included in the AHEAD (though vortex shedding does not lead to a *harmonic* excitation). However, as already discussed, vortex-shedding frequencies are most difficult to assess on the current knowledge base. Also, they cannot be attributed to a distinct mode shape. Parker and Stoneman's (1985) investigations on an axial-flow compressor show that acoustic resonances triggered by vortex-shedding are restricted to circumferential mode orders lower than half the vane count of the vortex-shedding vane array. For centrifugal compressors such investigations are not available.

One example of the AHEAD is shown in Figure 16. All frequencies are evaluated in the rotor frame of reference. Each AHEAD is valid for one given mode shape ($m_{TS}=m_{ac}=m_{struct}$). Frequency in the impeller frame of reference is plotted on the *x*-axis versus engine speed on the *y*-axis. The red vertical line(s) indicate the structural eigenfrequencies of the impeller, which are assumed to be constant for different rotor speeds (stiffening effect neglected). The black lines give the excitation frequency due to Tyler/Sofrin modes in the rotor frame of reference according to Equation (9). The first black line (steepest slope) corresponds to the rotor fundamental, the following black lines to higher rotor harmonics. The blue-bounded shaded regions indicate the acoustic

eigenfrequencies in the rotor frame of reference. Those frequencies (due to varying speeds of sound) depend on the compressor operating-condition. A practical example on how to derive the shaded regions will be given in the next section. As already mentioned, vortex-shedding (VS) is also included in the diagrams. Three different vortex-shedding mechanisms are taken into account: vortex-shedding from the compressor blades, vortex-shedding from the LSD vanes (if existent), and vortex-shedding at the side-cavity inlet. Operating conditions that are considered critical are characterized by a triple coincidence between Tyler/Sofrin excitation, structural eigenfrequency, and acoustical eigenfrequency. The graphical interpretation is an intersection point between the black and the red line within one of the blue-bounded shaded regions. Analogously, in terms of a critical operating point due to vortex shedding, the corresponding vortex shedding excitation regions must cross the red line of the structure within one of the shaded acoustic areas.

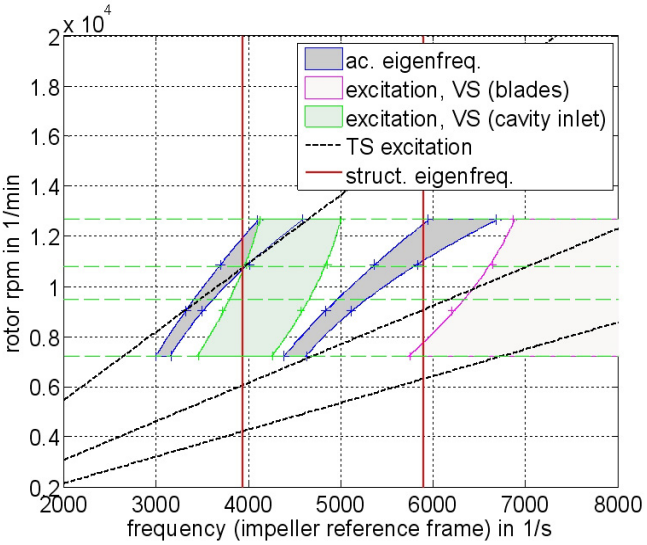


*Figure 16. AHEAD: Illustration of a Critical Operating Point and Root Cause of Impeller Failure.*

In Figure 16 the AHEAD is shown for an example where a critical operating condition occurs for the fifth nodal diameter. In this case a triple coincidence between Tyler/Sofrin excitation, acoustic eigenfrequency, and structural eigenfrequency is assumed to be the root cause of an impeller failure. The detailed root-cause analysis will be discussed in the next section. In the diagram the two red vertical lines indicate the first two structural eigenfrequencies of the fifth nodal diameter impeller mode. The first of these lines exhibits an intersection point with the first black Tyler/Sofrin excitation frequency line at 10,738 rpm. This black line corresponds to the Tyler/Sofrin mode with the same number of nodal diameters as the structural eigenmode. In the current case this mode is generated due to the fundamental interaction between 17 impeller blades and 22 return guide vanes, leading to $m_{TS}=1\bullet17-1\bullet22=-5$. The intersection point at 10,738 rpm is located within one of the two shaded acoustic regions. This region belongs to a coupled acoustic side-cavity eigenmode with five nodal diameters and no node circles ($m_{ac}=-5$, $n_{ac}=0$). If the compressor is operated close to 10,738 rpm the resulting resonance may lead to strong impeller vibratory stresses, which, in the current case, are assumed to have led to a failure of the impeller. Of no importance for the root-cause analysis at hand is the second shaded acoustic region located at higher frequencies, which corresponds to the acoustic mode with five nodal diameters and one node circle ($m_{ac}=-5$, $n_{ac}=1$). The two shaded regions that are left in the diagram are the frequency ranges due to vortex-shedding: The magenta-bounded region belongs to the frequencies caused by vortex-shedding from the impeller blades, and the green-bounded region to the frequencies due to vortex-shedding at the side-cavity inlet. The lower frequency boundary of the latter indicates that the acoustic resonance may also be triggered by a cavity-related vortex-shedding phenomenon. However, as already discussed, the uncertainties of the vortex-shedding frequencies are too large to allow definite conclusions. On the other hand, the estimated frequencies caused by vortex-shedding from the impeller blades are way too high to cause an acoustic resonance, even if large uncertainties in Strouhal number are allowed.

The AHEAD gives a composite picture of a possible impeller excitation due to aeroacoustic phenomena for a given circumferential mode order. However, some open questions remain. First of all it is unclear which acoustic modes are most relevant for impeller excitation. With this respect, it must be clarified if mode orders that are higher than half the blade count—it is common practice to limit the analysis of bladed assemblies to modes with nodal diameters smaller than $z_B/2$—may lead to impeller failures. Some failure patterns indicate that such higher-order modes may be of relevance though they are ignored by current analysis procedures. It all coalesces to the question of the relevance of the different phenomena with respect to their amplitudes: How strong are the amplitudes due to rotor/stator interaction? What amplitudes are necessary to excite an acoustic resonance? How strong are the resulting pressure amplitudes of such an acoustic resonance? And many more. Only dedicated experiments can give answers to those questions. The authors are optimistic that the basic experimental investigations that are ongoing will shed light on the complicated phenomena. A completely different aspect is the determination of reliable Strouhal numbers for engine-representative flow conditions. Only if such information is available, can a reliable prediction of vortex-shedding-related excitation phenomena become possible.

## ROOT-CAUSE ANALYSIS OF A FAILED IMPELLER WITH RESPECT TO AEROACOUSTIC PHENOMENA

Lots of theory has been presented in the preceding sections to enlighten the AHEAD methodology. In this section, one practical application of the AHEAD to explain the root cause of the fifth stage impeller failure of a five-stage high-pressure centrifugal compressor is given. For a detailed description of the compressor under consideration and the respective impeller failure see the beginning of this paper.

### *Speed of Sound and Real Gas Behavior*

Acoustic resonances are one key aspect of the AHEAD evaluation procedure, whereupon the respective acoustic eigenmodes are strongly dependant on the prevailing speed of sound: If the influence of flow is neglected, the acoustic eigenfrequency is directly proportional to the speed of sound (compare Equation [10]). The speed of sound, on the other hand, is a function of the compressibility factor $Z$, the isentropic exponent $\kappa$, the gas constant R, and the temperature:

$$a=\sqrt{Z\kappa RT} \tag{18}$$

For real gases the compressibility factor $Z$ and the isentropic exponent  are functions of temperature and pressure. $Z$, $\kappa$, and R include the influence of the gas composition. Since the speed of sound depends on temperature and pressure, it is a function of the operation condition of the compressor.

For the high-pressure compressor under investigation real gas effects are very pronounced: $Z$ and $\kappa$ both exhibit a strong dependency on temperature and pressure. Within the compressor speed range the variation of $\kappa$ and $Z$ may take values up to 40 percent and 25 percent, respectively. Considering Equation (18) this behavior leads to a complicated nonlinear function $a=f(T, p)$, which is illustrated in Figure 17.

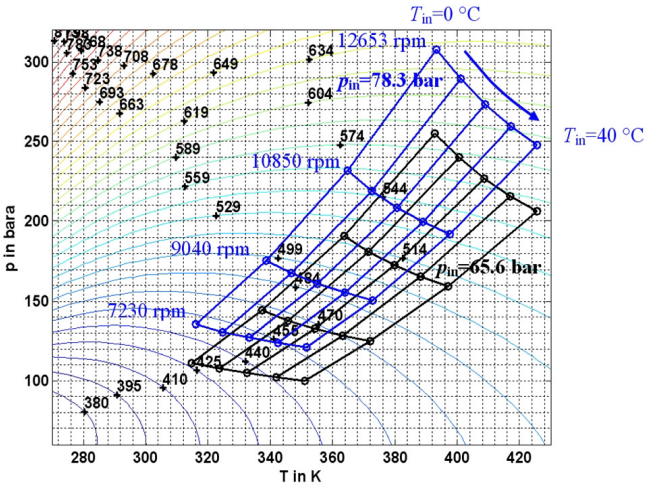


*Figure 17. a(p,t)-Dependency for Given Gas Composition.*

Isolines of constant speed of sound are marked by a cross and a label indicating the corresponding speed-of-sound value. Furthermore, approximate (*T*-*p*)-pairs at the impeller outlet of the fifth stage, resulting from different compressor inlet conditions and different compressor speeds, are included in the $a(T, p)$-map. The blue set of lines corresponds to a compressor-inlet pressure of 78.3 bar (1136 psi) (the maximum pressure from the compressor specification data sheet) and the black set of lines to a compressor-inlet pressure of 65.6 bar (951 psi) (the minimum pressure from the compressor specification data sheet). Within the two sets of lines, four different compressor speeds ranging from 7230 rpm (minimum continuous speed) to 12,653 rpm (maximum continuous speed) are covered. Furthermore, the resulting operating points for four inlet temperatures, covering the range from 0°C (32°F) to 40°C (104°F), were calculated. The calculations of the approximate operating points were carried out with in-house compressor-prediction tools. From the slope of the isolines in connection with the map of the operating points it can be seen that no clear tendency toward a minimum or maximum speed of sound value for given rotor speed can be given as a function of inlet temperature or pressure. For example, in Figure 17, the minimum speed of sound for 7230 rpm (427 m/s [1401 fps]) occurs at $p_{in}$ =65.6 bar (951 psi) and $T_{in}$ =0°C (32°F) whereas the minimum speed of sound for 12,653 rpm (554 m/s [1818 fps]) occurs at $p_{in}$ =65.6 bar (951 psi) and $T_{in}$ =40°C (104°F). Similar observations can be made for the maxima of the speed of sound for given rotor speed. However, all maximum speed-of-sound values occur at the highest inlet pressure, whereas all minimum speed-of-sound values occur at the lowest inlet pressure.

From Figure 17 the compressor inlet conditions $p_{in}$ and $T_{in}$ corresponding to the maximum and minimum speeds of sound for a given rotor speed were determined for stage five of the compressor (the stage where the failure occurred) and those input parameters were applied as boundary conditions for the more accurate calculation with in-house compressor-design tools. The resulting speed-of-sound range is the basis for the blue-bounded shaded acoustic eigenfrequency regions in the AHEAD (compare Figure 16).

As can be seen for the current example, the inclusion of the operating-point dependency of the speed of sound is crucial when investigating acoustic eigenmodes in centrifugal compressors. However, a representation in tabular form would result in a confusing quantity of numbers that do not allow an assessment of the inherent model inaccuracies. The AHEAD, on the other hand, gives a clear picture on the acoustic eigenfrequency behavior and the graphical representation allows a visual impression of the influence of a variation in speed of sound.

*Coupling Analysis*

For the root-cause analysis based on the AHEAD methodology, three main steps are necessary to investigate a possible coupling between structural eigenmode, acoustic eigenmode, and Tyler/Sofrin mode:

1. The structural eigenmodes and the corresponding eigenfrequencies must be determined. This may be achieved by finite element calculations or experimental modal analyses. In the current case, due to the failed impeller, no experimental investigation could be carried out; the frequencies and mode shapes were calculated numerically. However, an empirical correction of the calculated frequencies was applied, based on experience from comparisons between calculated and measured values.

2. The acoustic eigenmodes and the corresponding eigenfrequencies must be determined. Since an experimental identification is not feasible, the required information must be obtained theoretically. In the current case, a 3D finite-element model of the whole compressor stage was created and the results were compared with the 2D analytical model.

3. The Tyler/Sofrin modes that result from the interaction between stationary vanes and rotating blades must be determined. For the compressor under investigation 18 inlet guide vanes, 22 return guide vanes, and 17 impeller blades are the basis for the analysis.

For each circumferential mode order $m=m_{TS}=m_{ac}=m_{struct}$ one AHEAD was established for $-8 \le m \le 8$, incorporating the frequencies from items 1 to 3. In Figure 16 one example is given for $m=-5$. As already discussed, the red lines indicate the structural eigenfrequencies, the blue-bounded shaded regions the acoustic eigenfrequencies, and the black lines the Tyler/Sofrin excitation. The additional vortex-shedding excitation frequencies are based on Strouhal numbers, characteristic lengths, and local flow velocities from design calculations. For the vortex-shedding from the impeller blades a Strouhal number of 0.26 was assumed. The corresponding magenta-bounded shaded region results from geometrical uncertainties (varying trailing edge thickness). For the vortex-shedding at the cavity inlet a Strouhal number range from 0.35 to 0.45 was assumed, leading to the extended green-bounded shaded regions in the AHEAD. A detailed description of the diagram in Figure 16 was already given in the preceding section.

For the root-cause analysis two compressor speed ranges are of special interest:

1. 9500 rpm to 10,800 rpm: this is the speed range where the failures had occurred.

2. 7230 rpm to 12,653 rpm: this is the whole speed range according to the compressor design specification.

Both speed ranges are indicated in the AHEAD as horizontal dashed green lines (refer to Figure 16).

To assess the risk of aeroacoustic/structural coupling, an automated evaluation procedure has been established, that applies the AHEAD methodology to a variety of different vane counts. With this procedure, vane counts that may lead to a critical Tyler/Sofrin excitation can be identified. Of course, for root-cause analyses, the vane count is a given parameter.

The vane-count range follows from the circumferential mode orders under investigation, which, in the current case, span from −8 to +8. Only primary interactions ($h_B$=1, $h_V$=−1 in Equation [2]) between the blade and vane array are taken into account. For each vane-count the risk for aeroacoustic/structural coupling is evaluated the following way: The intersection point between the red line (structural eigenfrequency) and the first black line (fundamental excitation frequency) is determined and its distance

from the blue-bounded shaded region along a horizontal line of rpm=const. is calculated. If the intersection point lies within the shaded region, the risk for aeroacoustic/structural coupling is defined as "very high." If the relative-frequency distance between the intersection point and the blue-bounded shaded region is below 4 percent the risk is still assumed to be "high," due to the model assumptions described earlier. "Medium" risk is defined for a safety margin below 10 percent, and "low risk" for a safety margin greater or equal than 10 percent. If the intersection point between the red and the black lines lies outside the operating range of the compressor (<7230 rpm or >12,653 rpm) "no risk" for coupling exists, since no aeroacoustic/structural coupling can take place within the operating range. In Figure 18 labels are defined to indicate the different risk scenarios.

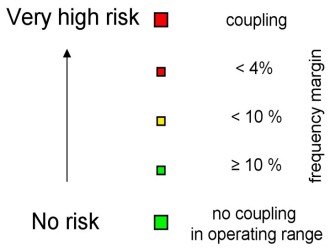


*Figure 18. Risk of Aeroacoustic/Structural Coupling.*

The results of the risk analysis are visualized in Figure 19. It can be seen that between 9500 rpm and 10,800 rpm (the speed range of the failed unit) critical coupling conditions may arise for vane counts of 21 and 22. The risk for the first one is considered "medium," whereas for the latter it is considered "very high." Taking into account the relevant vane count of the compressor under investigation ($z_{RGV}$=22), it becomes obvious that the current design is not acceptable if the new AHEAD methodology is applied: The interaction between 17 impeller blades and 22 return guide vanes produces the primary Tyler/Sofrin mode $m_{TS}$=1•17−1•22=−5, which leads to a critical coupling condition at 10,738 rpm. This scenario is visualized in the AHEAD in Figure 16. As already stated, the coupling between Tyler/Sofrin mode, acoustic mode in the side cavities, and structural eigenfrequency within the speed range of the failed compressor is assumed to be the root cause of the failure.

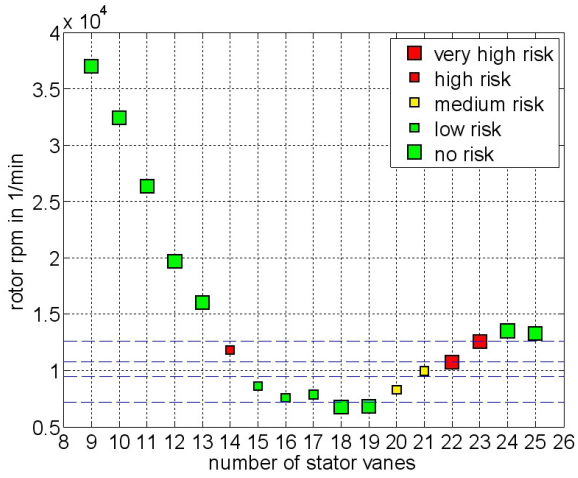


*Figure 19. Coupling Analysis for Different Vane Counts.*

*Acoustic Mode Relevant for Impeller Failure*

The mode shape of the acoustic eigenmode that is included in the root cause scenario mentioned above can be seen in Figure 20 to Figure 22 (the modulus of the pressure amplitudes is depicted). Red regions indicate high-pressure amplitudes and blue regions low-pressure amplitudes, respectively. Ten pressure-amplitude maxima indicating the fifth nodal diameter mode are clearly visible (no nodal circles are present). This acoustic mode shows a good correlation with the corresponding structural mode shape given in Figure 3 (right), leading to a strong mode-coupling (compare the illustration in Figure 15). It can be seen that the strongest pressure amplitudes occur in the shroud-side cavity—remember that it was the shroud disk that failed—but the mode is fully coupled between both cavities. Note that the *amplitudes* of the pressure fluctuations are shown (modulus). If the sign of the pressure waves in the two cavities is considered, it is important to consider that the sign changes from one cavity to the other: both waves are in counter phase. This leads to locally fluctuating net axial forces on the impeller.

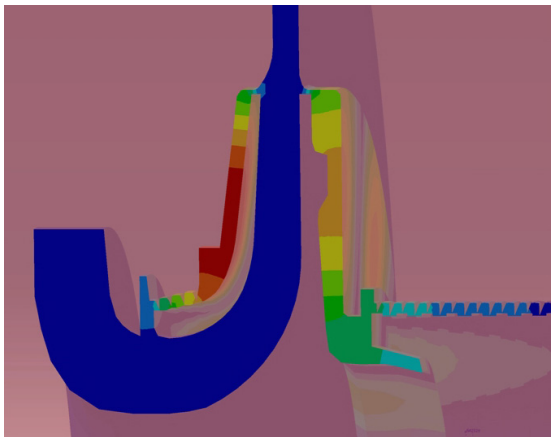

*Figure 20. Coupled Acoustic Side-Cavity Eigenmode ($m_{ac}$=−5).*

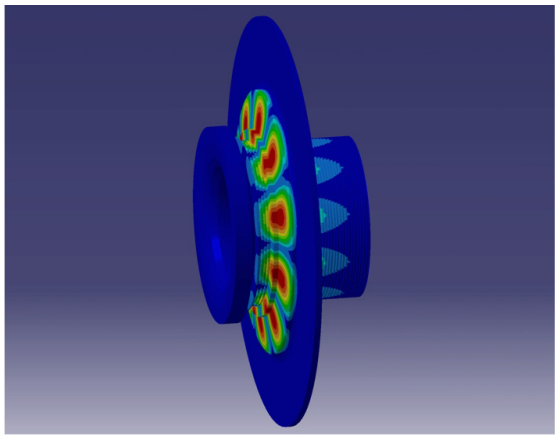

*Figure 21. Coupled Acoustic Side-Cavity Eigenmode ($m_{ac}$=−5); View on Shroud Side.*

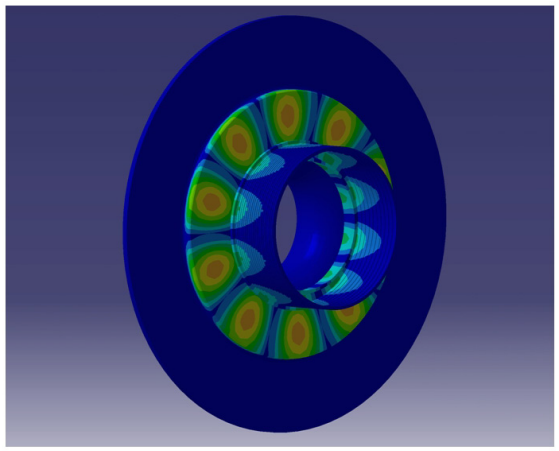

*Figure 22. Coupled Acoustic Side-Cavity Eigenmode ($m_{ac}$=−5); View on Hub Side.*

From a numerical point of view, the calculation of the whole compressor stage requires high modeling and computational efforts. To minimize the influence of geometrical uncertainties even the labyrinth seals were included in the current analysis. This domain was chosen based on the results of fundamental investigations presented in König (2009). In Figure 20 it can be seen that the acoustic mode extends—at least partly—beyond both labyrinth seals. No relevant pressure amplitudes occur at the domain-confining boundaries and within the impeller. This implies that geometrical uncertainties due to the current model are negligible. Of course, the swirl correction discussed earlier must be considered if the calculated frequencies are included in the AHEAD.

It is interesting to note that, though the 3D calculation reveals a complicated coupled mode system, a root-cause analysis based on the simple 2D-model presented earlier in the paper would lead to the same root cause of the impeller failure. For $m_{ac}=-5$ the deviations between the calculated frequencies are below 5 percent, which, due to the spread of the acoustic shaded regions included in the AHEAD, lead to triple coincidences for both calculation procedures. Certainly, this is partly due to the cancellation of some effects for the analytical model, but it shows that this simple model is at least useful for a first-guess estimate. Considering the time-efforts for both approaches under the assumption that the structural eigenfrequencies are known in advance—a few minutes for the analytical estimate stand versus several days for the 3D-modeling plus calculation—it must be carefully evaluated if a complete 3D-analysis is necessary to obtain the required accuracy in an industrial context.

*New Design and General Remarks*

After the failure had occurred, an immediate remedy was demanded from the operator to avoid a failure of a second, very similar compression unit operated in the same field. Based on a preliminary analysis with the analytical acoustical model in combination with the calculated structural eigenfrequencies, the approximate critical speed range could be determined within a few days. This speed range was excluded from the operating range of the compressor and subsequent damage could be averted.

After this preliminary calculation, a detailed root-cause analysis was carried out. At this stage the knowledge base was rather limited compared to the expertise that we have today. Though the analytical model was used for this first root-cause analysis and nothing was known about the necessity of the swirl correction, a design solution could be found that avoids critical triple coincidences within the whole compressor-operating range. For this design solution the number of return guide vanes was changed from 22 to 25, and the application of the AHEAD methodology revealed that triple coincidences can be avoided with the new design for all compressor stages. The interaction with the inlet guide vanes was also included in this evaluation. For the failed compressor stage, Figure 19 shows that "no risk" occurs for the new design with 25 return guide vanes. Similar diagrams were derived for all stages and the new design was found to be safe, regardless of uncertainties in the calculation of the acoustic eigenfrequencies. The new design was accepted from the operator and is currently being installed. Due to its simplicity the new design solution was especially appealing: no rotating parts are affected and the return guide vanes could be exchanged with relative ease. This case is a typical example that shows that a basic understanding of the underlying mechanisms is necessary to attack practical problems occurring in the field, and, more importantly, to avoid such problems in future designs.

## APPLICATION OF THE ROOT-CAUSE ANALYSIS TO A SECOND IMPELLER-FAILURE CASE

Due to promising outcome of the root-cause analysis presented in the preceding section, the AHEAD methodology was applied to try to explain a series of impeller failures that occurred in 2003/2004: after a revamp in 2002, three identical five-stage natural-gas compressors failed within a period of only a few months (failures B1, B2, and B3). The failure patterns showed strong similarities to the failure presented in the preceding section (compare Figure 23 for failures B and Figure 1 for failure A).

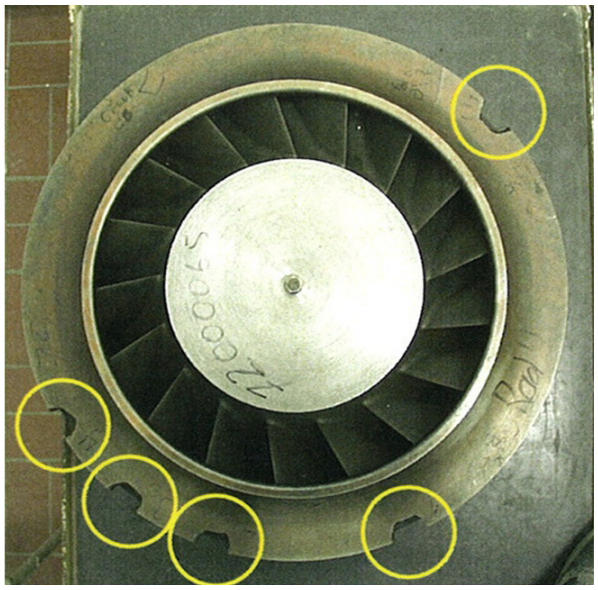

*Figure 23. Fatigue Failure on the Shroud of Stage Two (Failure B).*

The blade and vane counts were identical for failures B and failure A (17 rotor blades, 18 inlet guide vanes, and 22 return guide vanes). Compressors B were operated at lower pressures (design suction pressure of 4.8 bar [69.6 psi]) than compressor A (design suction pressure of 65.6 bar [951 psi]). Whereas it was the last (fifth) stage that failed for compressor A, it was the second stage for compressors B. Compressor A was equipped with 2D blading and compressors B with 3D blading.

The case of the failure B compressors was closed in 2004 and a design change was carried out by means of a reduction in the return-guide-vane count from 22 to 19. At that time, neither the OEM, nor the operator, nor independent consultants could derive a conclusive root cause of the failures. Nevertheless, after the design change, all three units have been running without problems ever since. This clearly indicates that the root cause of the failures must be related to the number of return guide vanes.

Though the problem of the case B failures could be solved with a pragmatic solution, it is the OEM's philosophy to understand the *origin* of the problems that occur in the field. Only this approach enables continuous improvement and increased operational availability of the machines. For this reason the investigation of past impeller failures is one main aspect on the way to a reliable aeroacoustic excitation model. In this section, as one example, the case-B impeller failures are subject to a root-cause analysis. Only the main findings of this analysis are presented; indepth results would go beyond the scope of this paper.

The same methodology as for the impeller failure presented in the preceding section was applied for case B. Two different root-cause scenarios could be derived. The corresponding AHEADs are given in Figure 24. The structural eigenfrequencies (red lines) were obtained from an experimental modal analysis of a spare impeller. The blue-bounded shaded regions of the acoustic eigenfrequencies were calculated with the finite-element method including the whole failed compressor stage; they are corrected with a swirl factor of 0.5. The first root cause scenario depicted in Figure 24 (left) is based on a critical coupling condition for $m=m_{TS}=m_{ac}=m_{struct}=-5$ at 8785 rpm. At this rotor speed a coincidence between mode shapes and frequencies occurs if an

uncertainty of the acoustic eigenfrequency of only 3 percent is allowed for. The corresponding acoustic and structural mode shapes are shown in Figure 25 and Figure 26 (left). The second root-cause scenario depicted in Figure 24 (right) is based on a critical coupling condition for $m=m_{TS}=m_{ac}=m_{struct}=-3$ at 8481 rpm. Again, this coupling condition occurs if an uncertainty of less than 3 percent is allowed for the acoustic eigenfrequency. The corresponding acoustic and structural mode shapes are given in Figure 25 and Figure 26 (right).

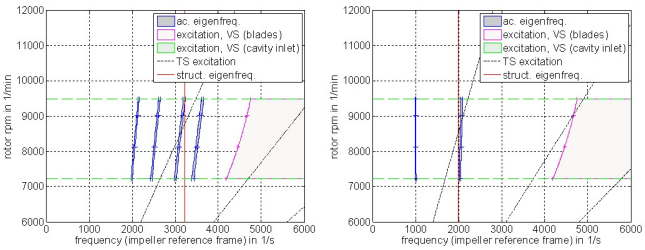


*Figure 24. AHEADs for Second RCA (Left: m=−5, Right: m=−3).*

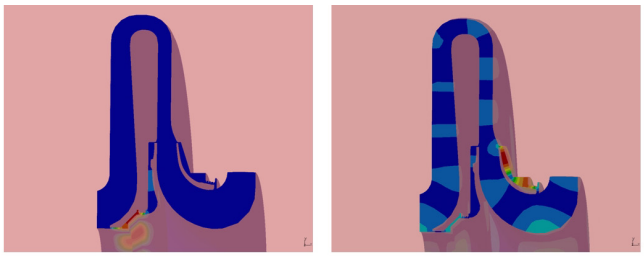

*Figure 25. Acoustic Eigenmodes Included in Second RCA (Left: $m_{ac}=-5$, Right: $m_{ac}=3$).*

*Figure 26. Structural Eigenmodes Included in Second RCA (Left: $m_{struct}=-5$, Right: $m_{struct}=3$).*

As can be seen in Figure 25, both acoustic mode shapes included in the root-cause scenarios are not solely determined by their number of nodal diameters. The $m_{ac}=3$ mode in the right-hand figure is located in the shroud-side cavity and characterized by one nodal circle. The maximum pressure amplitudes occur in the regions where the maximum structural displacements are expected (compare Figure 26 [right]). This leads to a strong coupling-effectiveness between acoustic and structural mode. The $m_{ac}=-5$ mode, on the other hand, is mainly located beyond the labyrinth of the hub-side cavity. The corresponding coupling-effectiveness is very small, even though the fifth nodal diameter character of this mode also occurs in the shroud-side cavity. However, the resulting amplitudes on the shroud disk are too small to be resolved in Figure 25 (left).

Both root-cause scenarios are based on harmonic fluid dynamic excitation due to Tyler/Sofrin modes, as indicated by the black lines in Figure 24. Vortex-shedding phenomena can be ruled out as excitation sources, since the estimated frequencies, even if large uncertainties in Strouhal numbers are allowed, are way too high. The Tyler/Sofrin modes that lead to the relevant excitation lines in Figure 24 are given in Table 5. It can be seen that $m_{TS}=-5$ results from the primary interaction between impeller blades and return guide vanes. This is assumed to be the strongest rotor/stator interaction pattern. Much weaker excitation amplitudes are expected for $m_{TS}=3$: for the generation of this mode the fundamental (first harmonic) of the return guide vanes and the second harmonic of the inlet guide vanes must be accounted for. The test-rig results presented earlier in this paper indicate that such interactions may indeed excite acoustic resonances with the same circumferential mode order; however, the direct excitation of the impeller structure due to such a pressure pattern is negligible.

*Table 5. Tyler/Sofrin Modes Included in Second RCA (Compare Equation [8]).*

| $m_{TS}$ | $h_B$ | $h_{RGV}$ | $h_{IGV}$ |
|---|---|---|---|
| -5 | 1 | -1 | 0 |
| 3 | 1 | 1 | -2 |

From the investigation of the second impeller-failure case presented in the current section it can be summarized that two root-cause scenarios can be derived if the AHEAD methodology is applied. The operating data made available from the operator do not allow a clear indication as to which scenario is the more likely. The $m=-5$ case is characterized by the stronger Tyler/Sofrin excitation pattern, but exhibits a very weak coupling-effectiveness between the mode shapes. The $m=3$ case, on the other hand, seems the more likely scenario if the corresponding acoustic resonance in the shroud-side cavity constitutes the dominant impeller-excitation source. In this case, however, the question remains as to whether the amplitudes due to rotor/stator interaction are strong enough to trigger a critical acoustic resonance condition. This illustrates that the AHEAD approach is a valuable tool to carry out root-cause analyses of impeller failures; however, more insight into the interaction mechanisms is needed before such a procedure can be used at the design stage of a compressor.

As already mentioned, the new design with 19 return guide vanes has been in operation since 2004 without any problems. It is important to note that the application of the new AHEAD methodology is consistent with this practical observation and evaluates the new design to be safe within the whole operating range.

## SUMMARY AND CONCLUSIONS

Centrifugal compressors have been subject to extensive studies over the past few decades. The machines have continuously improved with ever-growing efficiency values and increasing operational availability. Today, they can be considered as robust and technically mature systems that work reliably in a variety of different environments. However, in some very rare cases, compressor failures occur that cannot be explained with state-of-the-art analysis procedures. In such cases, a pragmatic remedy must usually be found at short notice, without really understanding the origin of the problem. This situation is quite unsatisfactory—for the operator and the OEM as well.

Aeroacoustic phenomena are suspected to play a critical role in the root causes of several impeller failures that have occurred within a timeframe of many years. Those failures could not be unambiguously explained, either by the operator, or the OEM, or independent consultants. The only way out of this dilemma is a better understanding of the relevant physics, since the current knowledge-base for aeroacoustic phenomena in centrifugal compressors is rather limited. For that reason, an extended in-house research program has been launched to address the involved interactions that may lead to machine failures.

The aim of the current paper is threefold: First, the excitation mechanisms that may be relevant for impeller failures are addressed. New insights from the OEM's research activities are

included. These activities cover detailed experimental investigations, transient CFD simulations, 3D finite-element acoustic analyses, and analytical modeling approaches. The second focus of the current paper is the practical conversion of the underlying theory into an aeroacoustic excitation model. The development of a methodology that includes the interaction between rotor/stator interaction patterns (Tyler/Sofrin modes), acoustic eigenmodes in the side cavities, and the impeller-structural eigenmodes is explained in detail. The interactions can be visualized in terms of so-called acoustic harmonic excitation analysis diagrams (AHEAD) to easily evaluate critical operating points. The third main aspect of the current paper is the application of the new methodology to two impeller failures in the oil and gas industry.

It can be summarized that the new methodology is capable of shedding light on the root causes of both impeller failures. The first failure, which occurred at the fifth stage of a five-stage natural-gas compressor, could be clearly attributed to an acoustic resonance in the shroud-side cavity of the last stage. For the second failure—which also occurred on a five-stage natural-gas compressor (but this time at the second stage)—two different root-cause scenarios could be derived. All scenarios are based on the interaction between an acoustic mode in the side cavities, the structural mode of the impeller, and the excitation due to Tyler/Sofrin modes. The critical operating points are characterized by a coincidence between mode shape (same number of nodal diameters for all three modes) and frequency.

Though the application of the AHEAD methodology gave promising results for the two impeller failures presented in the current paper, further research is necessary. Two new but important aspects have already been identified as crucial when calculating acoustic eigenmodes in the side cavities of centrifugal compressors. The first aspect is the inclusion of the real gas behavior of the speed of sound and its strong dependency on the compressor operating-point. The second aspect is the consideration of the fluid rotation in the side cavities. The latter postulation has been deduced from experimental results and will be investigated in more detail in future experiments.

The current paper is a step toward a better understanding of aeroacoustic excitation mechanisms in centrifugal compressors. The newly developed methodology is well suited to be applied in root-cause analyses. However, at the current stage, an implementation at the design stage is not yet feasible. The results clearly show that the very high efforts that are necessary to carry out fundamental experimental investigations are mandatory to make further progress in this challenging field of research. Today, powerful numerical tools are available and they constitute viable means for detailed studies. However, they cannot substitute dedicated experiments.

## APPENDIX A— FUNDAMENTALS OF FLOW INDUCED EXCITATION PHENOMENA

### *Surge*

If the mass flow of the overall system of the compressor varies with time, so that the entire compressor changes more or less in phase from being unstalled to stalled and back again, this behavior is called surge. Surge is a phenomenon of the whole system (including piping, valves, etc.) and not the compressor alone. The process may be so violent that the mass flow is reversed and the previously compressed gas emerges out of the inlet; this is sometimes called deep surge. The oscillations affect the power and axial-rotor thrust as well and, in the case of an uncooled compressor, will steadily increase the temperature level. The timescale for stall is much longer than for rotating stall. A detailed description of the phenomenon can be found in many textbooks (compare, e.g., Cumpsty, 2004; Lüdtke, 2004).

### *(Rotating) Stall, Rotating Instability*

Stall occurs when the flow locally separates, leading to regions of reversed flow. In the case of rotating stall, one or more stalled passages (stall cells) rotate around the circumference at a fraction of the rotor speed. The stall cells are characterized by having reduced or no through-flow. Different types of rotating stall exist in centrifugal compressors, the most common one occurring in vaneless diffusors.

Rotating stall can be regarded as a special case of a rotating aerodynamic instability as reported by Kameier (1993) and Kameier and Neise (1995). Unlike rotating stall, the pressure fluctuations of a rotating instability are unsteady in a frame rotating with the instability pattern. An observer moving with the instability cell would measure a discrete frequency signal associated with the pressure fluctuation, whereas, moving with the rotating stall cell, the pressure would remain constant. One can imagine a rotating instability as a rotating loudspeaker that is moving relative to the impeller in the circumferential direction. In a stationary frame of reference the rotating instability manifests, according to Baumgartner, et al. (1995), as a range of frequencies with a characteristic frequency signature; rotating stall, on the other hand, leads to a single discrete frequency with possible higher harmonics at most.

### *Vortex-Shedding from Bluff Bodies*

Though difficult to predict accurately, the formation of vortices shed from bluff bodies may lead to excitation forces due to pressure fluctuations caused by the vortices. The basic mechanism that determines the frequency of vortex-shedding behind any bluff body is the distance separating the two shear layers. This distance constitutes the characteristic length in Equation (1).

The simplest case of vortex-shedding from bluff bodies is the two-dimensional cylinder. Many investigations of vortex-shedding behind cylinders are available, and the behavior of the Strouhal number for this special case is well-known. However, for more complex geometries, e.g., a compressor blade, considerable scatter of the observed Strouhal number exists. For a flat plate the strong influence of the trailing edge profile on the Strouhal number was shown by Parker and Stoneman (1989). The influence of the axial spacing of blade rows on vortex-shedding was investigated by Parker and Stoneman (1987). Also, the vortex-shedding frequency may be influenced by acoustic resonances (compare Parker and Stoneman, 1989). Considering those aspects, excitation phenomena derived from vortex-shedding are subject to a great degree of uncertainty. Furthermore, due to the small pressure-fluctuations of the vortices, it is very unlikely that vortex-shedding alone will lead to fatigue failures. However, if a coupling between vortex-shedding and acoustic resonances takes place, high-pressure amplitudes may occur, eventually resulting in machine failures. Another case of special interest is the coincidence between vortex-shedding frequency and blade-passing frequency. The superposition of both effects could lead to increased pressure amplitudes.

In general, the vortex-shedding frequency from bluff bodies is influenced by the Reynolds number. For a cylinder, the lack of a clearly defined separation point on the surface of the cylinder makes the azimuth for a separating boundary layer more sensitive to the Reynolds number than for other geometries. For this case, the Strouhal/Reynolds number dependency can be found in Lucas, et al. (1997), for a wide range of Reynolds numbers. For the “supercritical” Reynolds number range, which is representative for the blades and diffuser vanes of typical high-pressure centrifugal compressors, they give a Strouhal number range between 0.17 and 0.45. This case is characterized by a narrow irregular wake downstream of the cylinder. The wide Strouhal number range illustrates that a compressor design that aims at avoiding excitation mechanisms due to vortex-shedding from blades and vanes is not practical with the current knowledge base. Experiments with engine-representative Reynolds numbers and geometries are necessary to obtain reliable Strouhal numbers for frequency-estimation purposes. This is one aim of the experiments that are ongoing.

*Vortex-Shedding at Cavities*

The flow past a rectangular or slotted cavity provides the basis not only for purely hydrodynamic self-sustained oscillations, but also the potential for the coupling of these basic instabilities with a resonant acoustic mode within the cavity or elastic characteristics of the cavity wall, compare Lucas, et al. (1997). They classify cavity oscillations as purely *fluid-dynamic*, *fluid-resonant*, and *fluid-elastic*. The latter phenomenon is characterized by elastic movement of the cavity-bounding walls and—due to the small fluctuation amplitudes of the solid component parts—is assumed to be less relevant for the centrifugal compressors under investigation. Fluid-dynamic oscillations alone are solely driven by the instability of the shear layer and the resulting pressure fluctuations are too small to lead to compressor failures. However, if a coupling with one or more acoustic resonant modes of the cavity takes places, strong amplitudes may result (fluid-resonant case).

A variety of cavity-oscillation models exist, one of the most prominent being the model of Rossiter (1964). From a feedback transit-time model and empirical estimates he derived the following formula for simple rectangular cavities:

$$\frac{fL}{U_\infty} = \frac{m_R - \xi}{1/K + M} \tag{A-1}$$

The left hand side of Equation (A-1) takes the form of a Strouhal number based on the cavity length $L$ and the free-stream velocity $U_\infty$. $f$ is the frequency of interest, $m_R$ denotes the stage of the Rossiter mode ($m_R$=1,2,3…), $\xi$ is an empirical constant, M the Mach number, and $K$ is the proportion of the free-stream speed at which the vortices travel over the cavity. $K$ is a constant and takes a value of 0.57, whereas $\xi$ depends on the length-to-depth ratio of the cavity. Rossiter's formula is valid for subsonic and transonic flow velocities. Many more models for cavity resonances are available, like the well-known Helmholtz resonator, whose mechanical analogon is a mass spring oscillator.

The application of such formulae for realistic geometries and flow conditions in turbomachinery is far from being straightforward. Typical examples are the side cavities of a centrifugal compressor, as depicted in Figure A-1. It can be seen that even the determination of a simple characteristic length is not obvious; in the current case the deviation between the two lengths L1 and L2 accounts for 60 percent, with the same influence on the predicted frequency. For other geometries the influence may be even stronger and the overall cavity geometry (in the simplest case a characteristic depth) must be defined as well. Even more challenging than the geometrical modeling is the determination of a representative free-stream velocity. The flow conditions in the depicted compressor region in Figure A-1 are extremely complex with time-dependant in- and outflow into the cavities. If the compressor is equipped with a vaned diffuser, the potential field of the low-solidity vanes located downstream leads to an additional dependency on the circumferential position. Considering those aspects, it becomes clear that even the application of more advanced methods, like the vortex blob method (for an overview on vortex methods compare Voutsinas, 2006), will lead to large uncertainties in the calculated frequencies. Values obtained with this method for simplified side-cavity geometries are occasionally stated to range between 0.35 and 0.6, but are at best a rough estimate for the prevailing frequencies. Furthermore, such a broad frequency range, which in some cases must even be extended, could excite a large variety of acoustic resonances. The use of such numerically determined Strouhal numbers for design purposes is not applicable, and even for root-cause analyses remains questionable. If the complex vortex-shedding mechanisms are to be implemented into the design process of centrifugal compressors, an experimental determination of the representative Strouhal numbers is mandatory and must be carried out for realistic geometries and flow conditions. Today such information is not available.

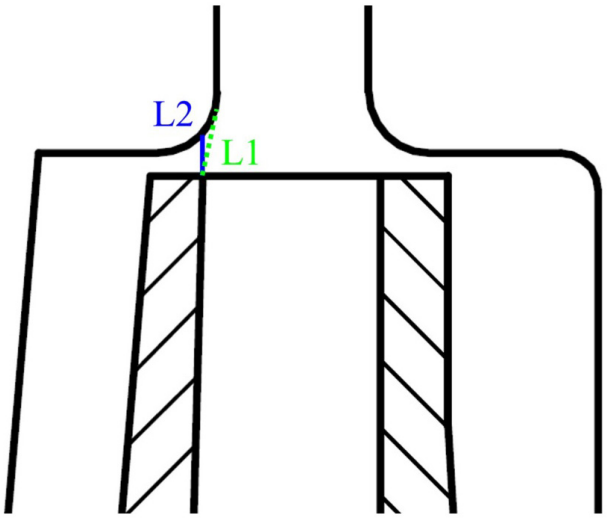


*Figure A-1. Impeller Outlet Region.*

*Side-Cavity Modes*

Acoustic eigenmodes in the side cavities of centrifugal compressors are assumed to play an important role in root-cause analyses of impeller failures that could not be explained by state-of-the-art evaluation procedures. They are also included in the root-cause analyses presented in the current paper. In open literature, no information is available on how to best model the side cavities by means of analytical correlations, or, more accurately, by means of finite-element methods. A recent study by König (2009) fills this gap. In the current paper some of the most relevant findings of this study are included.

In Figure A-2 the mode shape of a typical localized side-cavity mode is shown. The left-hand figure gives the pressure-amplitude distribution on the impeller shroud-disk, and the right-hand figure the corresponding pressure-amplitude distribution through the whole fluid domain for a fixed circumferential angle. The given mode shape is characterized by one nodal circle ($n_{ac}$=1). The 10 red regions on the circumference indicate the peaks and valleys (the modulus is depicted) of five complete acoustic wavelengths ($m_{ac}$=5), leading to a five nodal diameter structure. Several interesting aspects can be deduced from this figure:

1. The given mode extends over both cavities; hub- and shroud-side cavity are fully coupled.

2. The bladed impeller region and the region of the low-solidity vanes are not affected by relevant pressure amplitudes; their influence as well as the influence of impeller rotation can be neglected.

3. The given mode extends beyond some of the labyrinth spikes, but does not extend beyond the whole labyrinth.

Item 1 is valid for all modes of the given configuration (which corresponds to the test-stage depicted in Figure 8), but for some compressors the modes in hub- and shroud-side cavity are decoupled. Items 2 and 3 are not generally valid and must be verified for each mode separately. Item 3 strongly depends on the circumferential mode order: for higher mode orders, the influence of the labyrinth seal becomes more and more insignificant. A detailed analysis of all interesting aspects would be beyond the scope of this paper. More information on the relevant physics and the numerical modeling can be found in König (2009). One major point to be noted is the influence of flow rotation in the side cavities. For the current simulation a stagnant fluid was assumed, but the test-rig results indicate that a swirl correction is necessary

to obtain reliable eigenfrequencies. Since this aspect has not been considered in open literature so far, it is discussed in more detail in section AEROACOUSTIC EXCITATION MODEL FOR SIDE CAVITIES OF CENTRIFUGAL COMPRESSORS.

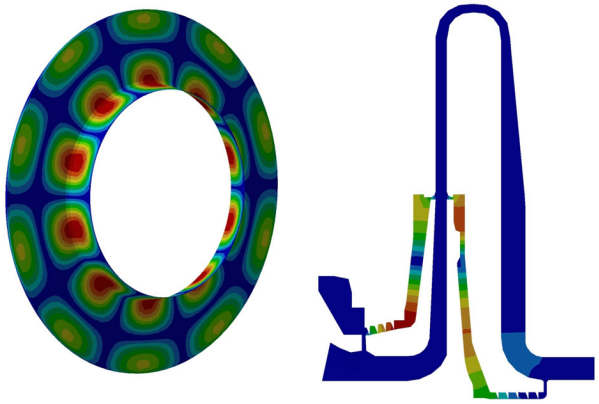

*Figure A-2. Side-Cavity Modes in Centrifugal Compressors.*

*Parker Modes*

Parker, in his fundamental studies on acoustic resonances (Parker, 1967a, 1967b, 1984; Parker and Pryce, 1974; Parker and Stoneman, 1985, 1987) found that acoustic resonances may be established that are localized to plate- or vane-arrays. To the authors' knowledge no such studies are available for centrifugal compressors in open literature. In principle, the typical Parker-type modes are possible for all vane- or blade-arrays, as long as a pitch-wise periodicity condition is satisfied (that is even number of blades or vanes), and if the chord-to-pitch ratio is sufficiently high. One component where Parker-type acoustic resonances are expected to be established in centrifugal compressors is the return-guide-vane cascade. An in-house empirical model has been developed that allows the calculation of the Parker-mode eigenfrequencies for typical return-guide-vane cascades. This model could in principle be applied at the design stage of the compressor; however, the excitation frequency (that is the vortex-shedding frequency from the vanes) is subject to large uncertainties. The test rig is instrumented in such a way that possible Parker-mode resonances can be detected. A systematic experimental study will be carried out to evaluate the resulting excitation amplitudes and to determine Strouhal numbers (that is, excitation frequencies) for realistic flow conditions in centrifugal compressors. Without this information, any conclusion drawn from calculations (whether simple analytic formulae or advanced 3D finite-element tools) is at best a rough estimate. It has to be noted that so far no Parker-mode acoustic resonances have been unambiguously detected in centrifugal compressors!

Some results of the preliminary numerical studies that were necessary to define the boundary conditions for the experiment are shown in Figure A-3 to Figure A-5. The red regions indicate high-pressure amplitudes (modulus) and the blue regions low-pressure amplitudes, respectively. Figure A-3 and Figure A-4 show mode shapes that exhibit characteristics of the original Parker modes (compare Parker, 1967b). Mode shapes of these types were identified by Parker for a cascade of flat plates. They are characterized by symmetry conditions in the plane of the flat plates or vanes, respectively. This means that the "pure" Parker modes can only be established for an even number of vanes. Of course, many more mode shapes are possible that are not restricted to a certain vane count. One example is shown in Figure A-5. As already mentioned, experimental investigations are necessary to verify the existence of Parker modes in centrifugal compressors. Especially for high pressure applications—due to the high Reynolds numbers—it is unclear if distinct vortex-shedding patterns are established downstream of the vanes; those are a prerequisite for the occurrence of the Parker modes.

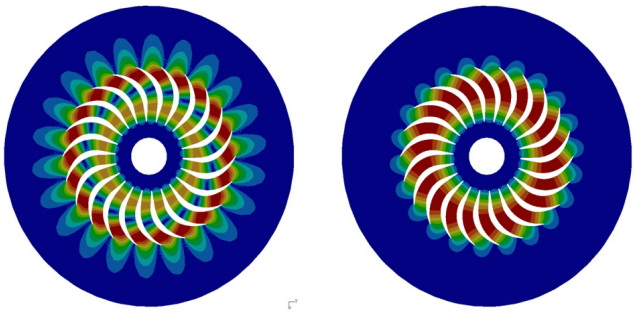

*Figure A-3. Parker Modes in RGV Cascade (Left: a-mode, Right: β-mode).*

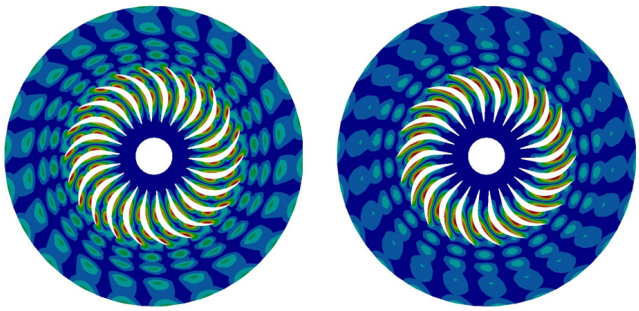

*Figure A-4. Parker Modes in RGV Cascade (Left: γ-mode, Right: δ-mode).*

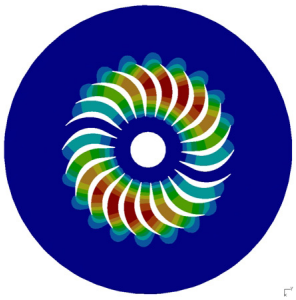

*Figure A-5. Typical Acoustic Eigenmode in RGV Cascade.*

REFERENCES

Baumgartner, M., Kameier, F., and Hourmouziadis, J., 1995, "Non-Engine Order Blade Vibration in a High Pressure Compressor," ISABE 95-7094, 1019-1030.

Cumpsty, N. A., 2004, "Compressor Aerodynamics," Krieger Publishing Company.

Eckert, L., 1999, "High Cycle Fatigue Cracks at Radial Fan Impellers Caused by Aeroelastic Self-Excited Impeller Vibrations, Part 1: Case History, Root Cause Analysis, Vibration Measurements," DETC99/VIB-8261.

Ehrich, F. F., 1969, "Acoustic Resonances and Multiple Pure Tone Noise in Turbomachinery Inlets," *ASME Journal of Engineering for Power*, pp. 253-262.

Eisinger, F. L., 2002, "Acoustic Fatigue of Impellers of Rotating Machinery," *ASME Journal of Pressure Vessel Technology*, *124*, pp. 154-160.

Eisinger, F. L. and Sullivan, R. E., 2002, "Acoustically-Induced Structural Fatigue of Impeller Discs—A Brief Note," ASME Paper GT-2002-30604.

Franke, G., Fisher, R., Powell, C., Seidel, U., and Koutnik, J., 2005, "On Pressure Mode Shapes Arising from Rotor/Stator Interactions," *Sound & Vibration Magazine*, *39*, pp. 14-18.

Kameier, F., 1993, "Experimentelle Untersuchung zur Entstehung und Minderung des Blattspitzen-Wirbellärms axialer Strömungsmaschinen," Ph.D. Thesis, DLR, Abteilung Turbulenzforschung, Berlin, Germany.

Kameier, F. and Neise, W., 1995, "Experimental Study of Tip Clearance Losses and Noise in Axial Turbomachines," (1186), Technical Report, VDI.

Kennepohl, F., Kahl, G., and Heinig, K., 2001, "Turbine Blade/Vane Interaction Noise: Calculation with a 3D Time-Linearized Euler Method," AIAA-2001-2152.

Lüdtke, K. H., 2004, "Process Centrifugal Compressors," Springer.

Lucas, M. J., Noreen, R. A., Sutherland, L. C., Cole, J. E., and Junger, M. C., 1997, "Handbook of the Acoustic Characteristics of Turbomachinery Cavities," ASME Press.

König, S., 2009, "Acoustic Eigenmodes in the Side Cavities of Centrifugal Compressors," ASME Paper GT2009-59650.

Ni, A., 1999, "High Cycle Fatigue Cracks at Radial Fan Impellers Caused by Aeroelastic Self-Excited Impeller Vibrations, Part 2: Mechanisms and Mathematical Model," DETC99/VIB-8262.

Parker, R., 1967a, "Resonance Effects in Wake Shedding from Compressor Blading," *Journal of Sound and Vibration*, *6*, pp. 302-309.

Parker, R., 1967b, "Resonance Effects in Wake Shedding From Parallel Plates: Calculation of Resonant Frequencies," *Journal of Sound and Vibration*, *5*, (2), pp. 330-343.

Parker, R. and Pryce, D. C., 1974, "Wake-Excited Resonances in an Annular Cascade: An Experimental Investigation," *Journal of Sound and Vibration*, *37*, (2), pp. 247-261.

Parker, R., 1984, "Acoustic Resonances and Blade Vibration in Axial Flow Compressors," *Journal of Sound and Vibration*, *92*, (4), pp. 529-539.

Parker, R. and Stoneman, S. A. T., 1985, "An Experimental Investigation of the Generation and Consequences of Acoustic Waves in an Axial Flow Compressor: Large Axial Spacings between Blade Rows," *Journal of Sound and Vibration*, *99*, pp. 169-192.

Parker, R. and Stoneman, S. A. T. (1987), "An Experimental Investigation of the Generation and Consequences of Acoustic Waves in an Axial Flow Compressor: The Effect of Variations in the Axial Spacings Between Blade Rows," *Journal of Sound and Vibration*, *116*, (3), pp. 509-525.

Parker, R. and Stoneman, S. A. T., 1989, "The Excitation and Consequences of Acoustic Resonances in Enclosed Fluid Flow around Solid Bodies," *Proc. Inst. Mech. Eng*., *203*, pp. 9-19.

Petry, N., Benra, K. F., König, S., and Woiczinski, C., 2009, "Interaction Between Aerodynamic Phenomena and Impeller Structure of High Pressure Radial Compressors," 8th European Turbomachinery Conference.

Rossiter, J. E., 1964, "Wind-Tunnel Experiments on the Flow over Rectangular Cavities at Subsonic and Transonic Speeds," *Royal Aircraft Establishment* (3438), Technical Report, Ministry of Aviation.

Schlichting, H., 1965, "Grenzschicht-Theorie," Verlag G. Braun.

Tyler, J. M. and Sofrin, T. G., 1961, "Axial Flow Compressor Noise Studies," *SAE Transactions*, *70*, pp. 309-332.

Voutsinas, S., 2006, "Vortex Methods in Aeronautics: How to Make Things Work," *International Journal of Computational Fluid Dynamics*, *20*, pp. 3-18.

Ziada, S., Oengören, A., and Vogel, A., 2002, "Acoustic Resonance in the Inlet Scroll of a Turbo-Compressor," *Journal of Fluids and Structures*, *16*, (3), pp. 361-373.